CORROSION RESISTANCE OF QUENCHED STEEL REBAR

BY

KHALED ALQAHTANI

A Thesis Presented to the

DEANSHIP OF GRADUATE STUDIES

KING FAHD UNIVERSITY OF PETROLEUM & MINERALS

DHAHRAN, SAUDI ARABIA

In Partial Fulfillment of the
Requirements for the Degree of

MASTER OF SCIENCE

In

MATERIALS SCIENCE AND ENGINEERING

JUNE 2015

KING FAHD UNIVERSITY OF PETROLEUM & MINERALS

DHAHRAN- 31261, SAUDI ARABIA

DEANSHIP OF GRADUATE STUDIES

This thesis, written by **KHALED ALQAHTANI** under the direction his thesis advisor and approved by his thesis committee, has been presented and accepted by the Dean of Graduate Studies, in partial fulfillment of the requirements for the degree of MASTER OF SCIENCE IN MATERIAL SCIENCE AND ENGINEERING.

Dr. Zuhair Mattoug Gasem
(Advisor)

Dr. Zuhair Mattoug Gasem
Chairman, ME

Dr. Mohammad Maslehuddin
(Member)

5/28/2015

Dr. Toor, Ihsanul Haq
(Member)

Dr. Salam A. Zummo
Dean of Graduate Studies

13/8/15

Date

Dedication

This work is dedicated to my lovely family

ACKNOWLEDGMENTS

I would like to thank my advisor Dr. Zuhair Mattoug Gasem and my committee members, Dr. Mohammad Maslehuddin and Dr. Toor, Ihsanul Haq for giving me this opportunity to learn and gain a good experience about the corrosion behaviour in steel rebar.

I am very grateful to all mechanical department personnels who spared some time to teach me and inform me about many activities and skills needed for this research. In addition I would like to express special gratitude to the researchers, engineers and technicians at Center for Engineering Research (CER) and Corrosion Center of the research Institute in KFUPM for their support and help as well as guidance during all the period of this research.

TABLE OF CONTENTS

LIST OF FIGURES

LIST OF TABLES

LIST OF ABBREVIATIONS

LPR	:	Linear polarization resistance
SCPS	:	Simulated concrete pore solution
E_{corr}	:	Corrosion potential (V)
I_{corr}	:	Corrosion current density ($\mu A/cm^2$)
SEM	:	Scanning electron microscopy
T	:	Temperature
^oC	:	degree centigrade
Fig.	:	Figure
*R*p	:	Polarization resistance
SCPS	:	Simulated concrete pore solution
PDP	:	Potentio-dynamic polarization
EDS	:	Systems include a sensitive x-ray detector, liquid nitrogen for cooling, and software to collect and analyze energy spectra.

ABSTRACT

Full Name : **Khaled ALQahtani**

Thesis Title : **Corrosion Resistance of Quenched Steel Rebar**

Major Field : **MATERIALS SCIENCE AND ENGINEERING**

Date of Degree : **JUNE 2015**

Corrosion of steel rebar is a major and very costly form of durability problem that threatens the performance of reinforced concrete structures, especially in an environment characterized with severe environmental conditions such as in the Arabian Gulf. Corrosion of reinforcing steel usually leads to spallation of the concrete layer which shortens the life-span of structures. This type of deterioration is principally attributed to de-passivation of the rebar steel due to chloride ions that might be contributed by the mix ingredients or diffused from the service environment.

The focus of this study is to investigate and compare the corrosion resistance of quenched steel rebar with air cooled steel rebar. The study was conducted in two parts. In the first part, mechanical tensile properties and corrosion resistance of quenched and air-cooled steel rebars obtained from various suppliers in the local market were characterized. The second part focused on investigating the corrosion resistance of different steel rebars microstructures that are produced by heat treatment encountered in steel rebar plants. The results indicate that the corrosion resistance of quenched and tempered microstructure is higher than bainite and perlite microstructures for the same steel composition. Tempering rebar sample at 400°C showed higher corrosion resistance than tempering at 300°C.

.

ARABIC ABSTRACT

ملخص الرسالة

الاسم الكامل :خالد عايض فيصل القحطاني

عنوان الرسالة: تآكل حديد التسليح الصلب

التخصص: هندسة مواد

تاريخ الدرجة العلمية: يونيو 2015

تآكل حديد التسليح الصلب هي المشكلة الرئيسية والأكثر كلفة في حديد التسليح وهي التي تهدد حاليا أداء المنشآت الخرسانية المسلحة، وخاصة في بيئة قاسية مثل ما هو موجود في منطقة الخليج العربي. تآكل حديد التسليح عادة ما يؤدي إلى سقوط طبقة الخرسانة مما يؤدي الى تقليل عمر البناء. ومما يسبب او يسرع هذا النوع من التآكل هو وجود أيونات الكلوريد التي يمكنها أن تساهم بتكسير الطبقة العازلة التي تكونت مع بداية التآكل.

محور هذه الدراسة هو مقارنة المقاومة للتآكل بين حديد التسليح المبرد بالهواء وحديد التسليح المبرد بالماء ومعرفة تأثير التبريد على تآكل حديد التسليح الصلب . وقد أجريت الدراسة على مرحلتين. في المرحلة الأولى، اخذ عينات من عدة شركات في المملكة العربية السعودية ودراسة مكوناتها ثم الحصول على معلومات عن ايهم مبرد بالماء او الهواء ثم مقارنة التآكل لكل نوع عن طريق غمرها في محلول يحاكي المحلول المائي للخرسانة ومعرفة كمية التآكل لكل عينة.

في حين الطريقة الثانية هي اخذ عينات حديد من نفس المادة وتسخينها ثم تبريده بفرن خاص لمحاكاة الخواص المجهرية لحديد التسليح للحصول على عدة عينات مختلفة الخواص المجهرية ثم دراسة التآكل لكل نوع.

تبين من هذه المقارنة ان تبريد حديد التسليح الصلب بالماء يزيد من مقاومة التآكل كما هو موضح في النتائج.

CHAPTER 1

INTRODUCTION

1.1 Reinforced Concrete Structures

Steel rebar is widely utilized in the construction of most of the facilities in Kingdom of Saudi Arabia. Concrete deterioration is noted in many of the structures since they are exposed to severe service conditions. The reduction in service-life in concrete structures is primarily due to corrosion of steel reinforcement. Concrete provides both chemical and physical protection to reinforcing steel. The chemical protection is provided by the highly alkaline nature of the fresh concrete pore solution (pH > 13), The physical protection to steel is provided by the dense and impermeable structure of concrete that retards the diffusion of aggressive species, like chlorides, carbon dioxide, oxygen, and moisture, to the steel-concrete interface. Reinforcement corrosion is caused by chloride ions that may be contributed by the mix ingredients or they may diffuse into the hardened concrete from the service environment. The extreme climatic conditions such as hot weather condition and the marginal quality of the aggregates accelerate concrete deterioration processes [1-3].

To reduce reinforcement corrosion of steel rebar, we need to use innovative methods, which are generally subdivided into two groups. First, deterioration or corrosion is slowed by extending the time for the chloride ions to reach the steel rebar. The second method aims to

spread the time between initiation of corrosion and the end of service life by using several techniques [4].

Deterioration of reinforced concrete in the coastal areas of the Arabian Gulf is often noted within a short span of 5 to 10 years. Field studies indicate that the deterioration of structures in this region is mainly attributed to: (i) inappropriate materials specifications, (ii) inadequate construction practices, and (iii) severe environment and geomorphic conditions. The environmental conditions of Saudi Arabia are characterized by a large variation in the daily and seasonal temperature. The ambient temperature in summer is as high as 45 to 55 °C and the relative humidity ranges between 40 to 95% over a period of 24 hours [5].

The temperature on the concrete surface at this ambient temperature may be as high as 70 °C due to solar radiation. The variation in the day to night temperature may be as much as 20 °C. This high variation in the day and night temperature leads to the formation of micro-cracks in the concrete that accelerate the diffusion of chlorides, moisture, oxygen and carbon dioxide, to steel surface thereby promoting corrosion of reinforcing steel. This corrosion is accompanied with substantial expansive force which leads to cracking in the concrete [6].

1.2 Research Objectives

The general objective of this study is to assess the corrosion resistance of steel rebars in concrete. The specific objectives are the following:

1. Study the corrosion resistance of various commercial rebars in the Saudi market.

2. Simulate the microstructure of Steel rebar by heat treatment experimentation.

3. Investigate the effect of microstructure on the corrosion resistance of steel rebars.

This thesis is divided into the following chapters. Chapter 1 is an introduction to the project highlighting the motivation and objective for the work. Chapter 2 is a literature review pertaining to the project. Chapter 3 details the experimental materials matrix and experimental design approach in order to achieve the project objectives. Chapter 4 presents the experimental results and discussion. Chapter 5 outlines the major conclusions from the study.

CHAPTER 2

LITERATURE REVIEW

2.1 Steel Rebar Process overview

Steel production process can be subdivided into iron making, steel making, steel casting, rolling (long products).

2.1.1 Iron Making

Direct Reduced Iron (DRI) is the primary raw material for steelmaking at the Electric Arc Furnace (EAF). The hot reducing gases, mainly Hydrogen and Carbon Monoxide (H_2 and CO), reduce iron oxide feed (Fe_2O_3), in form of pellets and/or lumps, in a vertical reactor termed Shaft Furnace. These gases are generated by reforming natural gas (CH_4) with recycled furnace outlet gases (CO_2 and H_2O), inside a catalytic reformer as shown in Figure 2.1 [7].

$$Fe_2O_3 + CO \rightarrow Fe + CO_2 \quad \text{.....2.1}$$

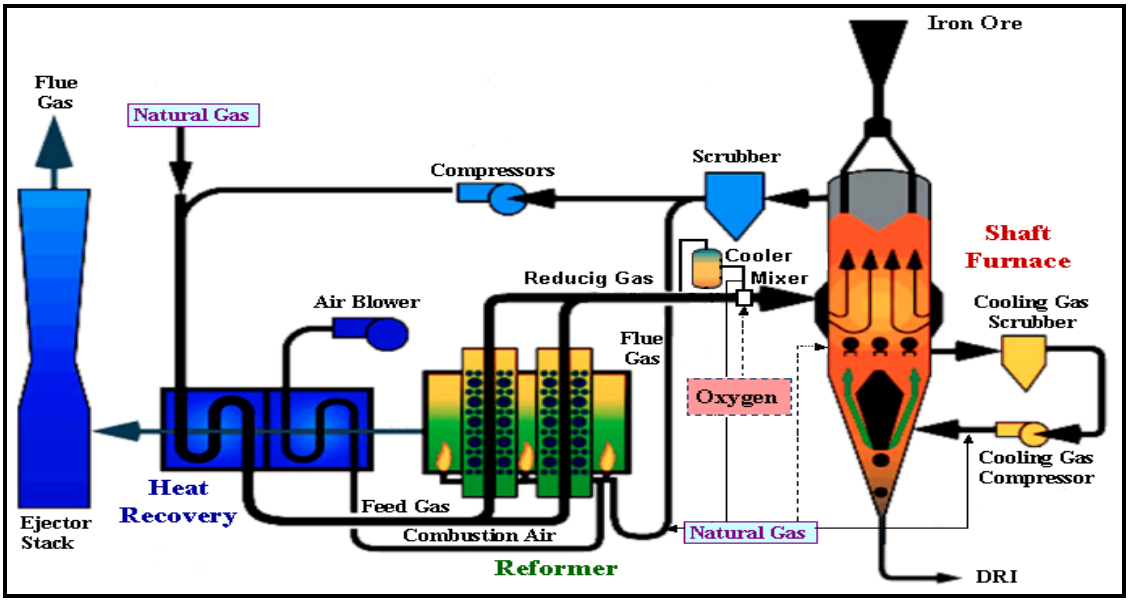

Figure 2.1: Midrex Direct Reduction Process Flow Sheet with Oxygen & Transition

2.1.2 Steel Making

Steel plant is the most important plant in all steel industries. Steel can be made through different processes. The steel can be produced in a basic oxygen furnace (BOF) where the main raw material for steel is hot metal from blast furnace. Steel production at Saudi Arabia is based on DRI, EAF and continuous casting route. Steel plant layout of is shown in Figure 2.2.

The electric Arc Furnace (EAF) is the units of steel making in which the electrical energy is converted by various methods into thermal energy for heating and melting the metal by heat radiated from three arcs according to the number of phases of alternating current.

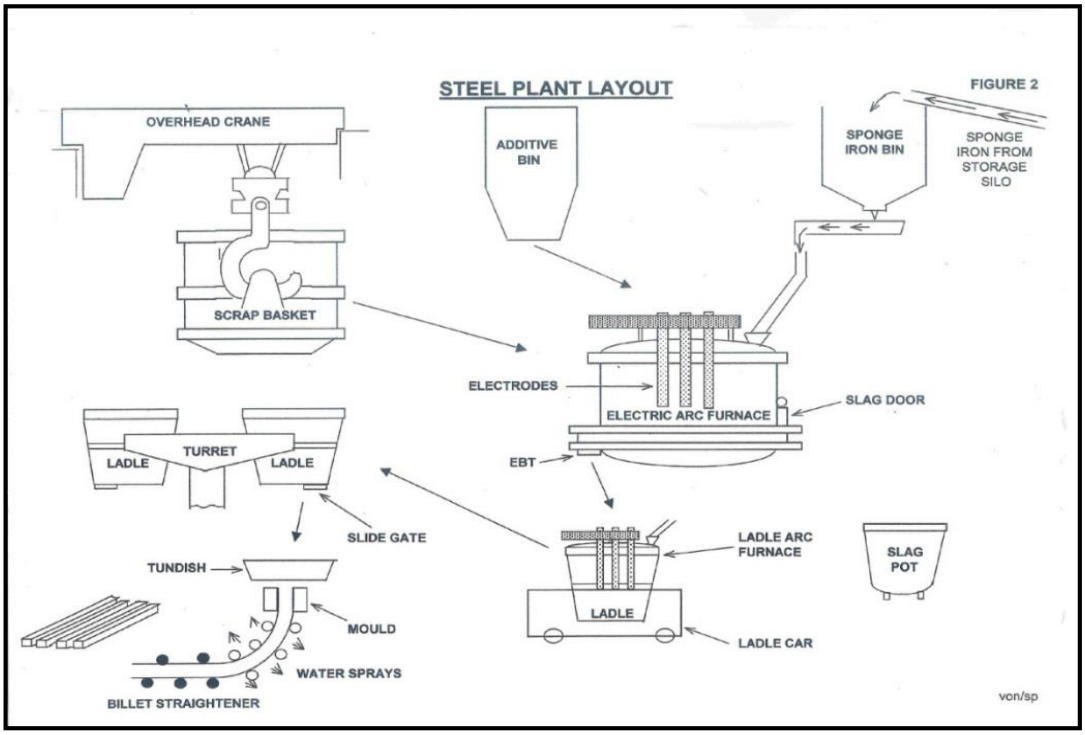

Figure 2.2: Steel Plant Layout

2.1.3 Steel Rolling

Steel rebar manufactures are divided into two processes based on the cooling methods. which is either cooling or water Quenching "Quenched and Self-Tempered". QST increases the strength of rebar due to the hard layer of surface "tempered martensite", as shown in Figure 2.3 [8]. Also, it reduces the cost of production due to reduction in the alloying. This technology has also been widely used to produce high strength rebar in Saudi Arabia.

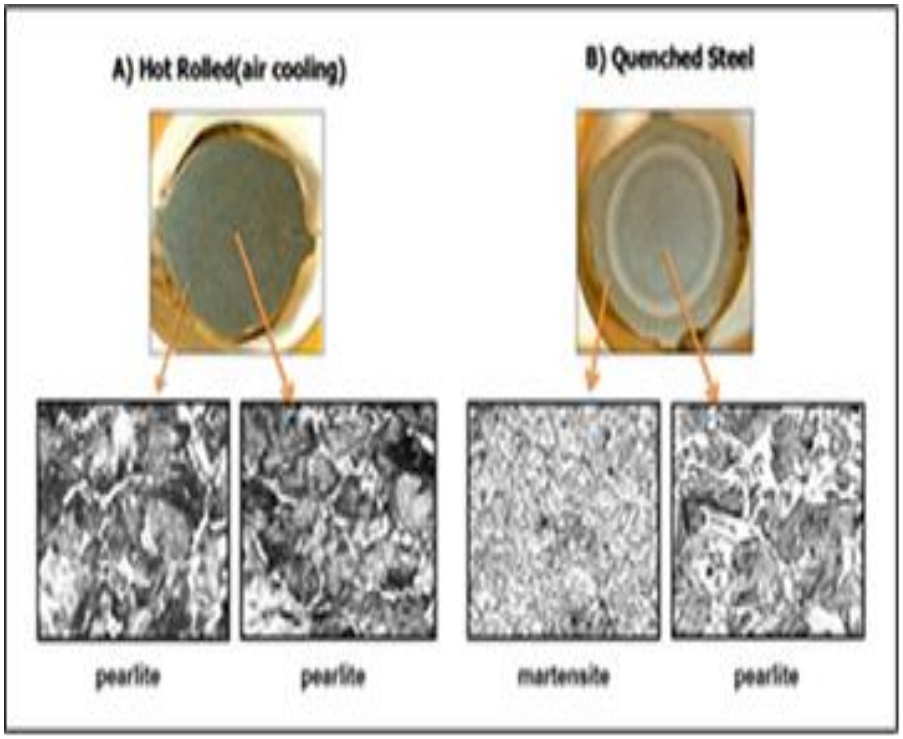

Figure 2.3: Microstructure of steel rebar (a) air cooling and (b) Water quenched.

The steel rebar is rolled at the continuous bar mill, where the heated billet is passed through a series of roll stands which gradually reduces the billet cross section. The deformation while reducing the cross section results in the elongation of the stock. The rolling stock can be several kilometer long depending upon the final size. Finally, the bar is cut to the required length for dispatch, as shown in Fig. [2.4].

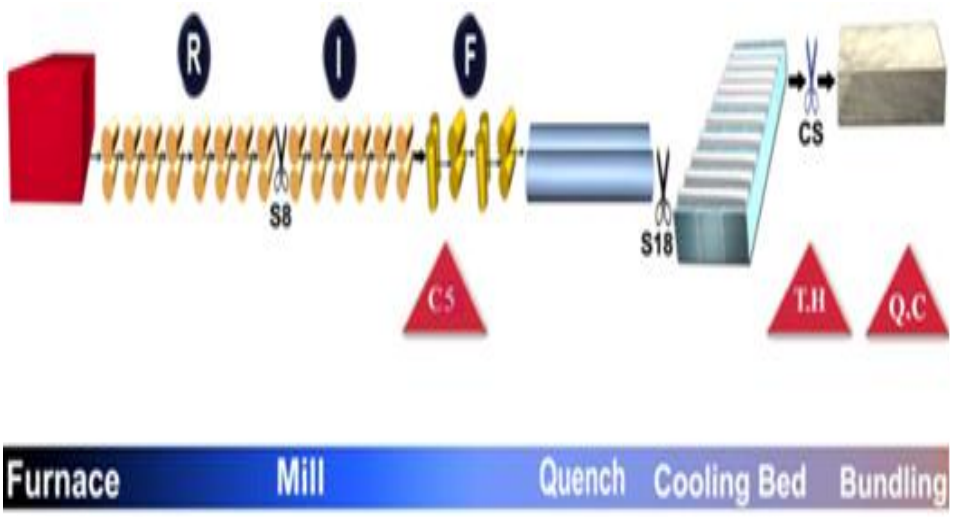

Figure 2.4: Steel bar rolling process

2.2 Corrosion Mechanism of Steel Rebar in Concrete

Corrosion of steel rebar in concrete is basically electrochemical process. Due to highly alkaline environment of concrete, a passive film layer grows on the steel surface which will protect steel rebar. On the other hand, the passive films gradually settle with the ingress of carbon dioxide or chloride ions within concrete cover. That will generate a potential difference between the active and passive regions at the steel surface. So, If the water and oxygen are close to the steel surface, the corrosion of steel rebar will start as shown in Figure 2.5. [14-23]

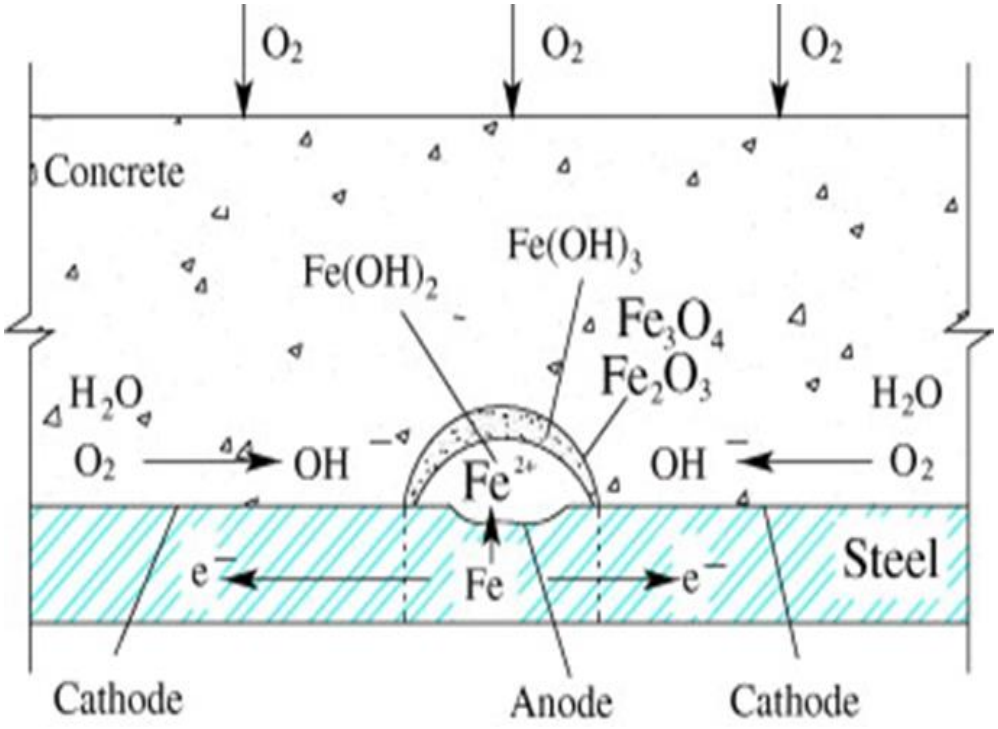

Figure 2.5: Corrosion of rebar inside the concrete [7].

The anodic reaction is given by:

$$Fe \rightarrow Fe^{2+} + 2\ e^{-} \quad \text{.....2.2}$$

The cathodic reaction is given by

$$O_2 + 4e^{-} + 2H_2O \rightarrow 4OH^{-} \quad \text{.....2.3}$$

Fe^{2+} and OH^{-} react with each other and form $Fe(OH)_2$ as shown in Equation (3).

$$Fe^{2+} + 2OH^{-} \rightarrow Fe(OH)_2 \quad \text{.....2.4}$$

If the oxygen supply is sufficient, $Fe(OH)_2$ will transform into $Fe(OH)_3$, which is large and porous, Fe_2O_3 is formed after dehydration, as shown in below in equation(4) and (5):

$$4Fe(OH)_2 + O_2 + 2H_2O \rightarrow 4Fe(OH)_3 \quad \text{..... .....2.5}$$

$$2Fe(OH)_3 \rightarrow Fe_2O_3 + 3\ H_2O \quad \text{.....2.6}$$

On the other hand, $Fe(OH)_2$ will transform into Fe_3O_4, if the oxygen is insufficient.

$$6Fe(OH)_2 + O_2 \rightarrow 2Fe_3O_4 + 6\ H_2O \quad \text{.....2.7}$$

Finally, corrosion of steel will cause expansion in the concrete due to volume expansion which leads to cracking of concrete cover and bond-slip between concrete and steel, as shown in Figure 2.6 [16].

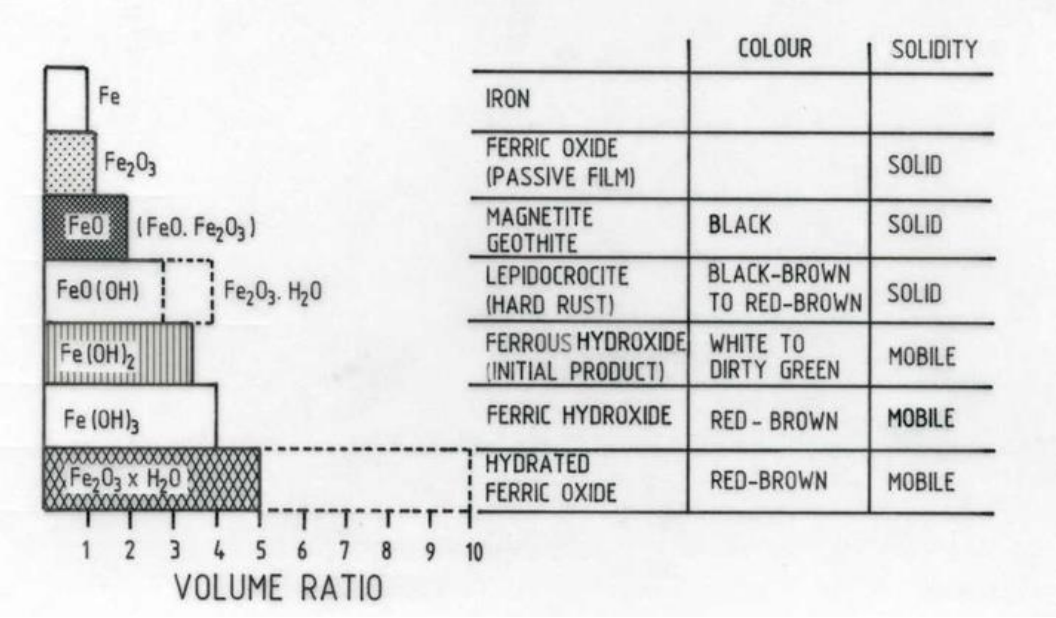

Figure 2.6: Volume of various oxides formed due to corrosion of iron [17].

2.2.1 Effect of treatment on steel Rebar

When carbon steel is quenched after heating, it will have martensite phase. It is a metasTable phase and it has body centered tetragonal lattice. So, the corrosion rate is relatively low for martensite in dilute acid. The carbon in interstitial position reacts with acid which will form a hydrocarbon gas which is observed as a black scale on the, steel surface [26].

In addition, tempered martensite form after heating martensite below 727 °C, then air cooling. The process called tempering which has cementite (iron carbide' Fe3C) and α iron ferrite. So, will have galvanic cells due to the two phase structure ferrite and iron carbide' that will accelerate corrosion rate. Also, the pearlite microstructure is formed after slow cooling of a carbon steel from 727 °C austenite which is face centered cubic lattice. Revie and Uhlig [26] claimed that "Corrosion rate of pearlite structure increases as the size of iron carbide particles decreases. Also, steels with fine pearlite structure corrode more rapidly than coarse pearlite structure and pearlite structure corrode more than spheroidized structure [27]. The importance of both the amount of cementite acting as cathode and its state of subdivision supports the electrochemical mechanism of corrosion [28].

2.2.2 Previous Studies on The Corrosion of steel rebar

Several researchers investigated the corrosion behavior of steel rebar by using several electrochemical methods. Mohamed et al 2013 and Evitts 2012 studied corrosion behaviour of steel rebars under chloride ions attack. Multiple electrochemical techniques were used with the aids of Gamry PC4 machine. A three-electrode corrosion cell was used for determining the corrosion characteristics and rates of the tested steel as shown in Figure 2.7.

They studied corrosion behaviour of stainless steel, micro-composite steel and carbon steel [26-27].

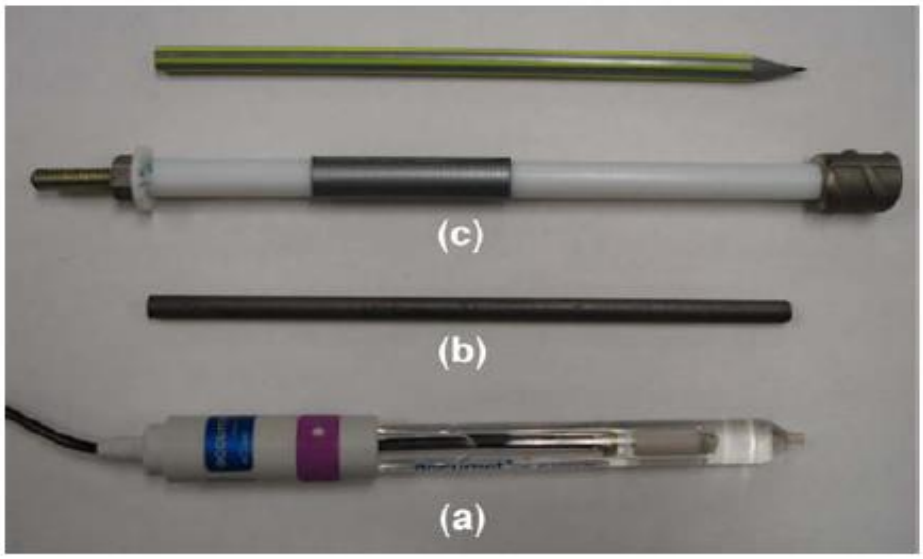

Figure 2.7: The electrodes used (a) reference electrode, (b) counter electrode,(c) working electrode attached to its holder[26]

While, Ghods and Miller [31-33] have experimentally investigated the effect of pore solution compositions on the protective properties of the oxide films of black reinforcing steel by using electrochemical impedance spectroscopy ”EIS” and polarization as shown in Figure 2.8.

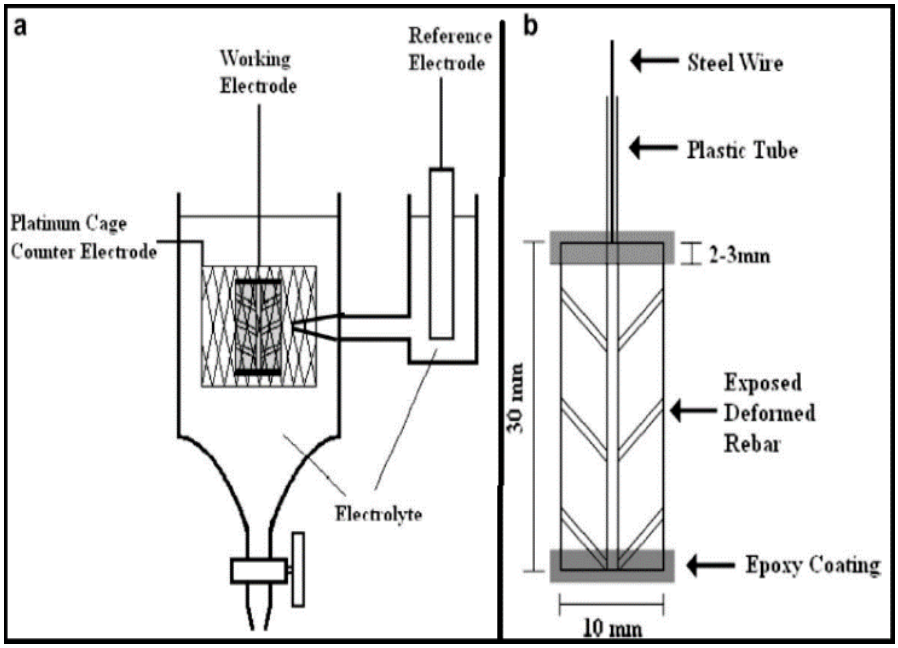

Figure 2.8: (a) Schematic for the setup of the test. (b) An illustration of the rebar samples preparation. [31].

2.2.3 Cooling processes effect on the corrosion of steel rebar

There is limited information about the corrosion of rebar, which are done by different cooling process. However, Wei and Dong [34-35] have experimentally investigated the influence of cooling on the corrosion resistance of the rebar. They compared the corrosion resistance of rebar cooled by Oil (FM), water quenching and air cooling. The results show that cooling by FM had higher corrosion resistance of the rebar electrode than that cooled by water or air as shown in Figure 2.9. Finally, the reason was that, the Fe_3O_4 content in the scale was around 60% for FM cooling; however, the Fe_3O_4 content is only 40% for water and air cooling [34-35].

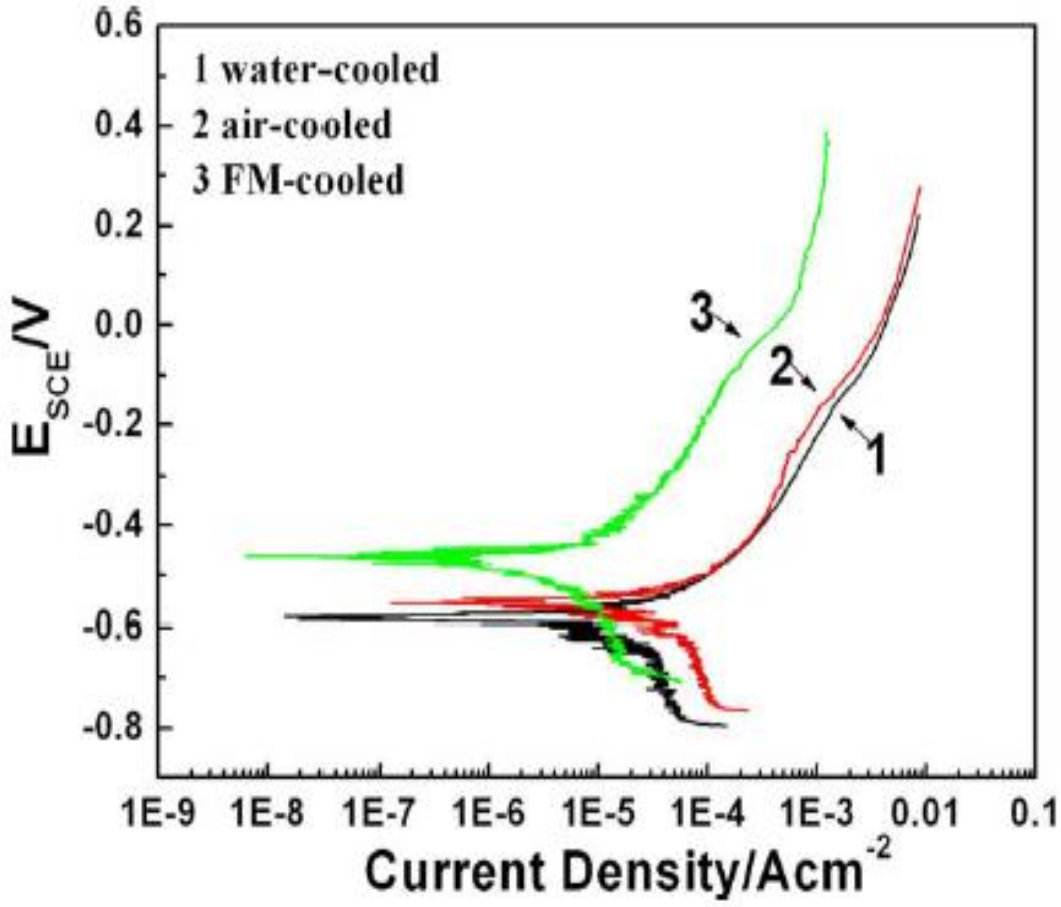

Figure 2.9: Tafel curves of rebar with water, FM and air cooling [34]

Zitrou and Nikolaou [36] evaluated the effect of reinforcing steel production method on the atmospheric corrosion resistance. These methods are air cooling "hot roll", air cooling with micro alloyed addition, Quenching "Tempcore" and work-hardened rebar by drawing process. The corrosion resistance was evaluated by measuring the thickness of the layer formed due to corrosion on the surface of the bars by using SEM as shown in Figure 2.10. They found that the work-hardened had the lower atmospheric corrosion resistance followed by Quenched rebar steel [36-37].

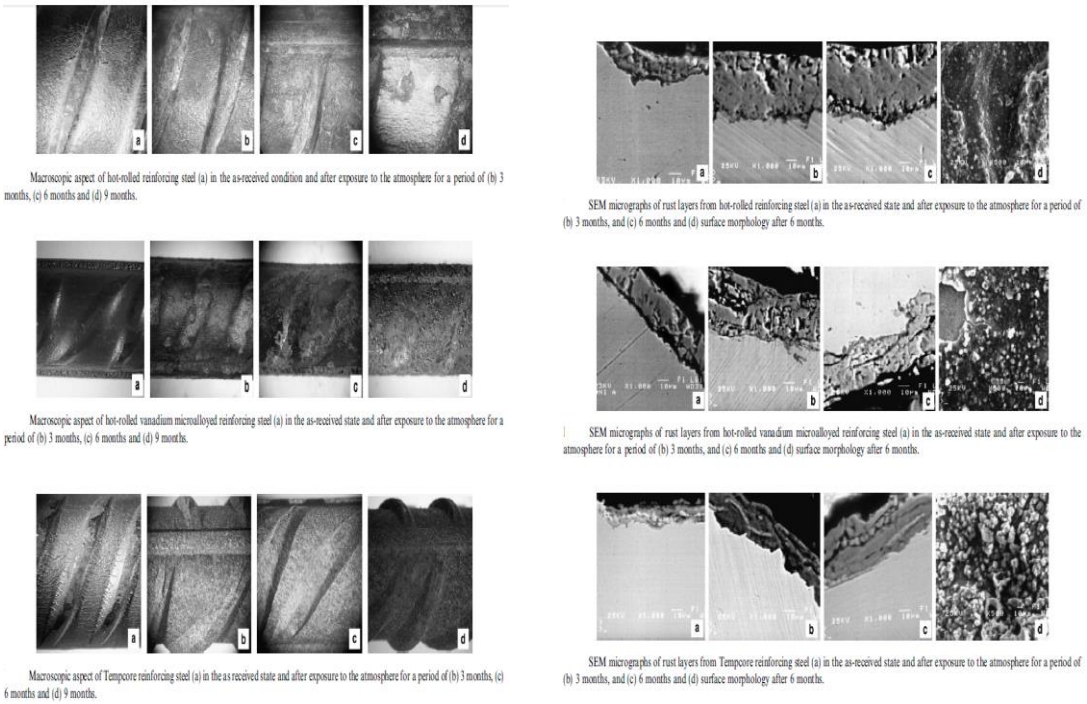

Figure 2.10: SEM micrographs of the layers due to rusting of steel after exposure periods of (a) as received (b) 3 months, (c) 6 months and (d) 9 months.[37]

2.2.4 Effect of Microstructure of Steel on the Corrosion Behavior Quenched steel

Mohammad [38] studied the performance of duel phase steel embedded in concrete with different volume fraction of martensite as compared to ordinary mild steel 0.161% C. The specimens were reheated in the furnace at the following annealing temperatures: 725, 735, 750, 770, 795, 815, and 840 ^{0}C for 20 minutes and then quenched in water in order to transform the austenite into martensite. The higher the intercritical annealing temperature, the higher the percentage of volume fraction of the martensite in dual-phase steels. After that, test specimens were initially cured in water for 14 days followed by accelerated corrosion curing in 3.5% chloride solution and sea water. From the Electrochemical

Corrosion - Tafel Extrapolation result as shown in Figure 2.11, it was observed, that the dual-phase steel rebar has better corrosion resistance if compared to the conventional steel rebar And he claimed that due to the presence of pearlite phase in the microstructure of conventional steel which contains the eutectoid carbide that is susceptible to pitting corrosion. On the other hand, dual-phase steel rebar is more corrosion resistant than conventional steel because it contains no carbide and most of the carbon atoms are trapped in the martensite structure.

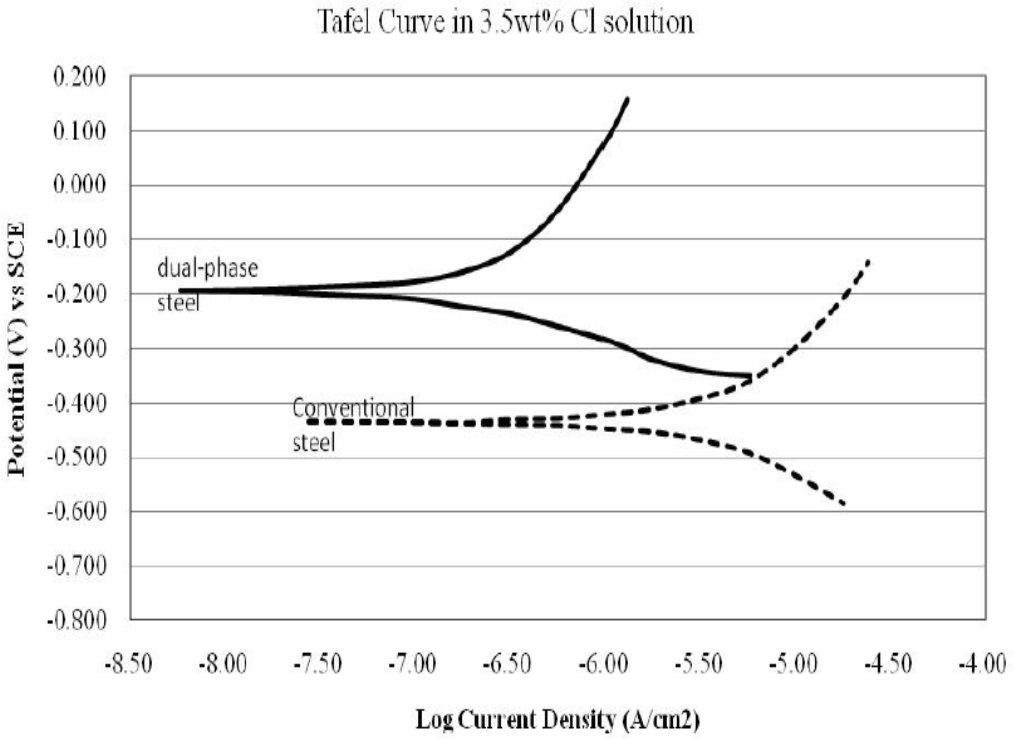

Figure 2.11: Tafel extrapolation curve of dual-phase steel and conventional steel in 3.5% wt in CaCl [38].

Paolinelli, Pérez and Simison [39] investigated pre-corrosion and steel microstructure in CO_2 corrosion with inhibitor performance. They used carbon steel with the following composition (wt%): 0.38 C– 0.99 Mn– 0.33 Si–0.17 Cr–<0.01 P–<0.01 S. They conducted two different heat treatments on the samples in a lab furnace. First, annealing (austenized at 890 C and furnace cooled – FP samples), and quenching and tempering (Q&T) (austenized at 890 C, water Q&T 1 h at 700 C – TM samples), after corrosion test they found TM has better corrosion resistance than FP as shown in the Figure 2.12 below. They claimed that the differences between the tempered martensite and the ferritic–pearlitic specimens could be related to their very different superficial iron carbide distribution.

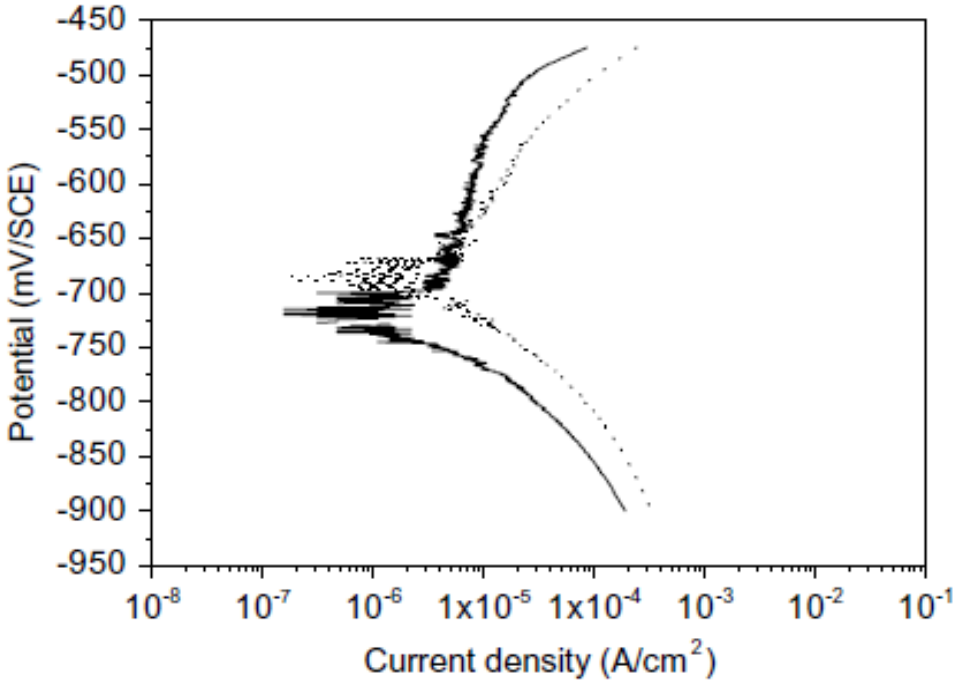

Figure 2.12: Comparison between polarization curves of TM (–) and FP (….) [39].

Bhagavathi, Chaudhari and Nath [40] studied corrosion behavior of plain low carbon steels with different volume fractions of martensite. Potentiodynamic polarization tests and immersion tests were conducted in 3.5% NaCl solution. These results are also compared with the corrosion behavior of as received steel with ferrite and pearlite as micro constituents. They found the corrosion rate which obtained from immersion test and potentiodaynamic test of DP(increase volume fractions of martensite) steel was less than SA(pearlite steel).The reason was the galvanic couple formed between ferrite and martensite is weaker than the galvanic couple formed between ferrite and pearlite.

Ramirez-Arteaga et al. [41] reported that with increasing the martensite percentage in the specimen and the ferrite percentage decreases the corrosion rate. For specimens quenched in water, the susceptibility to localized type of corrosion decreased by increasing the annealing temperature.

López et al. [42] described the influence of steel microstructure on CO_2 corrosion; They found tempered martensite samples to have a better corrosion resistance than the pearlite without inhibitor. So, the morphology of the cementite in each microstructure determines if such blockage is useful to reduce or to activate corrosion rate.

Clover1y et al. [43] investigated the influence of microstructure on the corrosion rate of various carbon steels. The samples were categorized according to four groups banded ferrite/pearlite microstructure, very fine predominantly ferrite microstructure, ferrite/coarser, and somewhat acicular pearlite/pearlite Microstructure and tempered martensite microstructure. It was found that steels with a banded ferrite/pearlite structure

perform poorly in terms of localized corrosion and this was attributed to a segregated distribution of the iron carbide phase cementite (Fe_3C). So, the distribution of cementite is responsible for the variation in corrosion performance.

Igwemezie and Ovri [44] contested in different corrosive ambience was carried out to study the effects of microstructural changes on the Corrosion resistance of Medium Carbon Steel .This has been done by heating the steel at 925 ^{o}C and cooling with various quench oil, water, and air to obtain normalized, annealed and martensitic microstructures. They claimed "the difference in corrosion rates due to precipitation of ferrite and carbide phases. So, these phases lead to setting up of microgalvanic cells within the microstructure with the carbide phase becoming cathodic and the ferrite anodic. Also, The result also tends to suggest that the more ferrite is precipitated (anodic area) in the normalized structure, the more corrosion rate increases. Furthermore, the higher corrosion rate in the martensitic structures was shown due to the combining effect of ferrite precipitation, transformation stress and carbide precipitation tends. This could be attributed to high metastability (non-equilibrum position) of martensitic structure. In general, normalized structure showed the lowest susceptibility to corrosion attack while the martensitic structure showed the highest susceptibility to corrosion attack.

Houyi and Chen [45] studied the effect of nitrate ions on the electrochemical behavior of iron (ferrite) and two carbon steels (martensite and pearlite) in sulphate solutions of different pH values. They have found the martensite has lower corrosion resistance as shown in the result below in Polarization curves and the charge-transfer resistance used to evaluate the

ability of resist corrosion. The smaller the charge-transfer resistance, the more easily is the material corroded. But, The samples used in this test has different chemical compositions.

Seikh [46] found the influence of heat treatment on the corrosion of microalloyed steel in sodium chloride solution. Corrosion resistance property of microalloyed steel has been studied with different microstructures conditions such as the three repeated quenched conditions. He found that with repeated heating and quenching recrystallization grains become finer, and corrosion rate increases. Samples heated to 600 ^{O}C just below the lower critical temperature (A3) than quenched.

Lucio-Garcia and Rodriguez [47] performed electrochemical techniques to study the effect of heat treatment on H_2S corrosion of a micro-alloyed C–Mn steel and the Microstructures was included martensite, ferrite, and ferrite plus bainite. All results showed that martensitic microstructure has highest corrosion rate. Also, for longer immersion times, the steel with a martensitic microstructure tended to exhibit a mixture of uniform and localized attack. They claimed that due to "the grain size and number of precipitated particles for steel with a martensitic microstructure was bigger than those for steels with a ferritic plus bainitic or ferritic microstructures. Furthermore, due to the fact that martensite grain boundaries are more reactive than ferrite or bainite, according to EIS results, the corrosion process was under charge transfer control. EN results showed that during testing the three steels were highly susceptible to a localized type of corrosion, with the exception of the steel with a martensitic microstructure, which had a higher tendency towards a mixture of uniform + localized types of corrosion at the end of the test.

Keleştemur and Yıldız [48] studied the effect of various dual-phase heat treatments on the corrosion behavior of reinforcing steel used in the reinforced concrete structures and SAE1010 structural carbon steel. They found that corrosion rate of dual-phase steel has increased with increase amount of martensite. So, they assumed this increase due to the variation in the morphology and distribution of the phase constituents. Since quenched treatment produces a very fine fibrous structure, it can be qualitatively said that the interfacial area between ferrite (cathode) and martensite (anode) is much more for quenched specimens compared to as received specimens resulting in higher corrosion rate for quenched treated specimen.

Al-rubaiey et al. from University of Technology in Baghdad [49] investigated the Influence of Microstructure on the Corrosion Rate of Carbon Steels. Four types of microstructures were obtained to study corrosion resistance for each. These microstructures are banded ferrite/pearlite microstructure, fine ferrite/pearlite microstructure, coarse ferrite/pearlite microstructure and tempered martensite microstructure. Mass loss and Optical microscopy used to study General corrosion and localized corrosion. Tempered martensite microstructures have higher localized pitting corrosion properties. Coarse ferrite/pearlite microstructures have better localized pitting corrosion resistances compared to others investigated microstructures. They claimed that corrosion happened with following mechanisms; (a) local anodes and cathodes may be formed due to electrochemical differences between matrix and secondary phases, and/or (b) scale may adhere preferentially to particular regions, due to factors such as carbide distribution, causing localized attack. Presumably, galvanic couples form between carbon-rich phases and the bulk steel, noting

that cementite is cathodic with respect to iron. This is consistent with suggestions made elsewhere that the shape and distribution of ferrite/Fe3C plays an important role in influencing the corrosion rate and pits shapes. Recent studies have shown that corrosion rate increases as the size of iron carbide particles decreases.

2.2.5 Effect of cooling processes on microstructure of steel rebar

Several researchers investigated the microstructure of steel rebar and compare it with mechanical properties. For example, Zaky and El-Bitar [50] have studied the effect of cooling by air or water on the mechanical properties of rebar. They investigated the microstructure by using SEM and optical microscopes. They found that water quenching to 600 ^{0}C and air cooling is the best regime showing the better mechanical properties [50].

On the other hand, Monideepa and Dutta [51] studied the hardness of the rim which is the tempered martensite of steel rebar by calculating the hardness of the tempered martensite as a function of temperature and the chemical composition [51].

CHAPTER 3

EXPERIMENTAL PROCEDURE

3.1 Experimental Approach

The assessment of steel rebar corrosion were evaluated by measuring the corrosion rate using potentiodynamic scanning and linear polarization techniques on steel specimens immersed in simulated concrete pore solution (SCPS). Furthermore, we simulate the microstructure of steel rebar by heat treatment experimentation and investigate the effect of microstructure on the corrosion resistance. This chapter gives information about the testing method, the materials included in the study and the selected heat-treatment schedules.

3.2 Materials

Four sets of rebar steels from different companies were selected for conducting corrosion test. Additionally, a set of rebar steel from one company was included in the study after heat treatment. The reason for including the additional set of rebar steel is to get the effect of microstructure on the corrosion resistance. Table 3.1 shows the chemical composition of these samples. Sample A, C and D were quenched and self-tempered and sample B was air cooled.

Table 3.1: Chemical compositions for four rebar samples in Saudi Arabia.

	SampleA	**Sample B**	**Sample c**	**Sample D**
Elements	Conc.%	Conc. %	Conc. %	Conc. %
C	0.2876	0.3659	0.2802	0.2701
Al	0.0177	Tracing	0.0186	0.0116
Si	0.1795	0.2405	0.1795	0.1770
P	0.0381	0.0373	0.0351	0.0366
S	0.0299	0.0293	0.0316	0.0223
Ti	0.0047	0.0046	0.0050	0.0063
V	0.0050	0.0040	0.0120	0.0057
Cr	0.0986	0.0529	0.1653	0.0351
Mn	0.6566	1.2541	0.6775	0.6243
Fe	Balance	Balance	Balance	Balance
Ni	0.0912	0.0428	0.0746	0.0247
Cu	0.2728	0.1358	0.0972	0.1070
Nb	0.0037	0.0078	0.0190	0.0073
Mo	0.0183	0.0072	0.0375	0.0073

3.2.1 Steel Specimens Design

Steel specimens of 28 mm length and 16 mm diameter were prepared and the surface of each sample was cleaned by using sand paper and acetone. Both ends of the steel samples were coated with epoxy resin, as shown in Figure 3.1. The top side of steel specimen was drilled to be fitted with coarse-thread stainless steel holder as shown in Figure 3.2 and Figure 3.3. The exposed area of the reinforcing steel was in the range of (14.50 to 14.75) cm^2.

Figure 3.1: The steel sample coated with epoxy

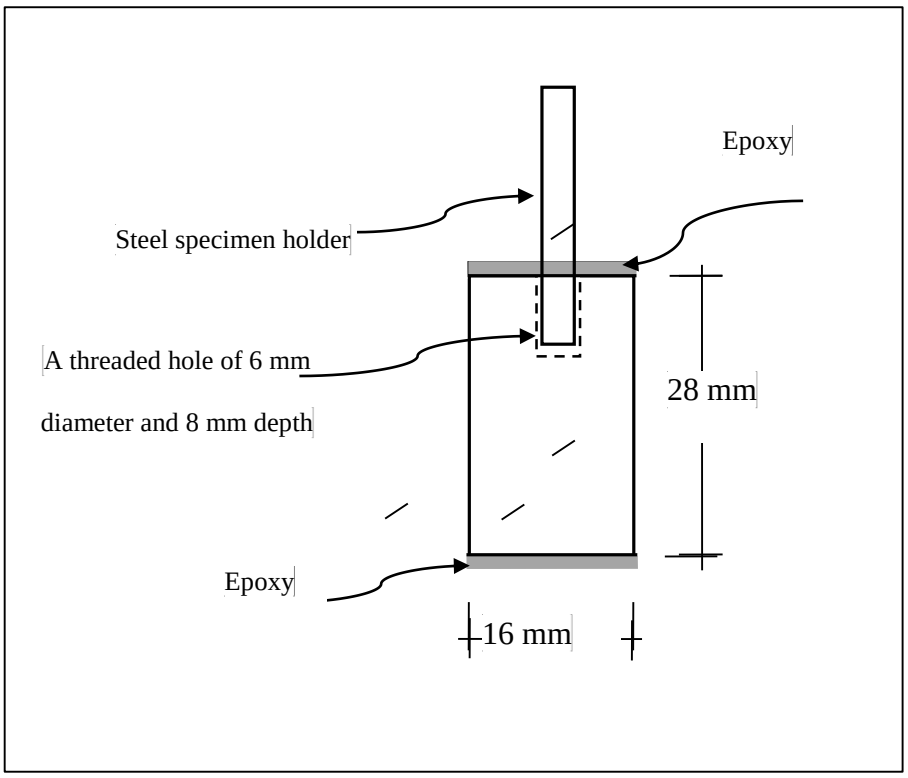

Figure 3.2: Schematic Representation of Steel Specimen preparation.

3.2.2 Simulated Concrete Pore Solution

The simulated concrete pore solution was prepared based on the analysis of concrete specimens at KFUPM which indicates that one liter of concrete pore solution contains 974 g of distilled water, 14 g of potassium hydroxide (KOH), 10 g of sodium hydroxide (NaOH), and 2 g of calcium hydroxide [$Ca(OH)_2$]. The simulated concrete pore solution has a pH of more than 13.4. Reagent grade chemicals of KOH, NaOH and Ca $(OH)_2$ were utilized to prepare the concrete pore solution. Figure 3.3 shows The simulated concrete pore solution.

Figure 3.3: The simulated concrete pore solution.

3.2.3 Description of the Corrosion Cell Preparation and Curing of Specimens

A three electrodes cell was used for the potentio-dynamic measurement. It mainly consists of three electrodes which are immersed in the solution as follows:

- Stainless steel plate was used as counter electrode.
- Saturated calomel electrode (SCE) used as the reference electrode.
- Working electrode (the tested steel specimen itself).

The steel samples were prepared as described in 3.2.1. In order to attach the steel specimen to the specimen holder, a threaded hole of 6 mm diameter and 8 mm deep was drilled in each sample. The specimen holder was covered with a Teflon tube to prevent any possibility of crevice corrosion. The electrolyte level was kept below the attaching point all the time. Figure 3.4 shows the working electrode, reference and counter electrode.

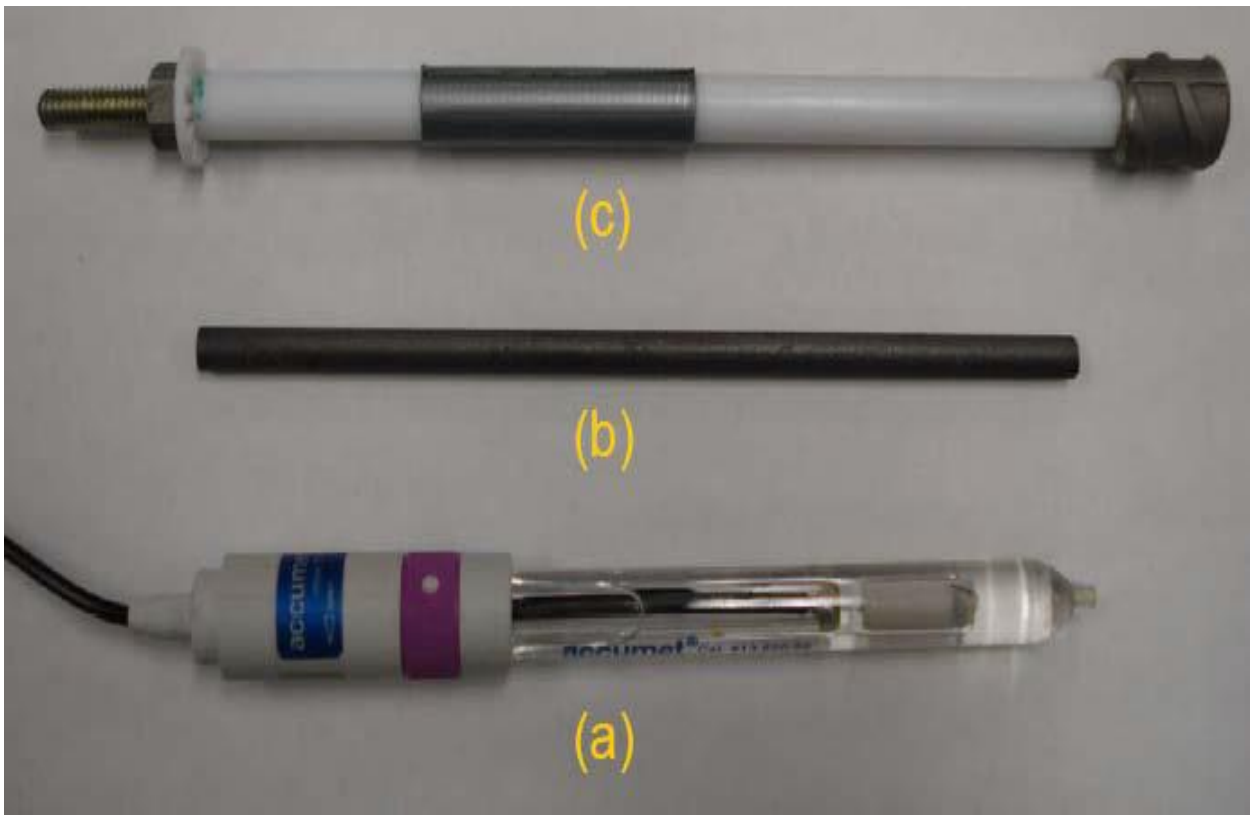

Figure 3.4: The Electrodes Used (a) Reference (b) Counter (c) working electrodes

3.2.4 Potentio-dynamic Testing

The potentio-dynamic method measures the current for a large potential sweep from the cathodic to the anodic region of the corrosion potential. The potentio-dynamic studies were conducted on bare steel exposed to electrolyte representing the concrete pore solution admixed with the selected inhibitors, selected chloride concentration and selected temperature. The potentio-dynamic potential-current curves were recorded by changing the electrode potential from -900 to +900 mV with a scan rate of 15 mV/minute, as shown in Figure 3.5. The schematic illustration in Figure 3.6 displays the main terminologies for a typical potentio-dynamic polarization diagram (PDP), which is plotted in terms of applied potential vs the logarithm of the measured corrosion current density. From this Figure, we can notice many futures which can be used to interpret the behavior of steel specimens under PDP test. The open circuit potential is located at Point (A) at which the sum of cathodic and anodic reaction on the working electrode is zero (often this point equals to corrosion potential). As the applied potential increases from A to B, anodic polarization moves to region (B), which is the passive region (increase in the applied potential without increase in the measured current). Point (C) is known as the active potential, and as the applied potential increases above this value, the current moves to region (D), which is called active region. At region (D), the current density increases with the increase in the applied potential and steel oxidation is the dominant reaction taking place. The increase in current continues with the increase in the applied potential till it reaches point (E), which is the limit point of anodic scan. In some cases, sudden increase in the measured current may be noted without an

increase in the potential, which indicates presence of pitting corrosion and the corresponding potential called the pitting potential, as shown in Figure 3.7.

In the cathodic scan, the applied potential increased in the negative direction, as anodic scan point (A) represents the open circuit potential. As the applied potential increases in the negative direction the current moves into region (F), which represents the oxygen reduction reaction (cathodic polarization). This increase continues till point (H), which is the limit point for cathodic scan.

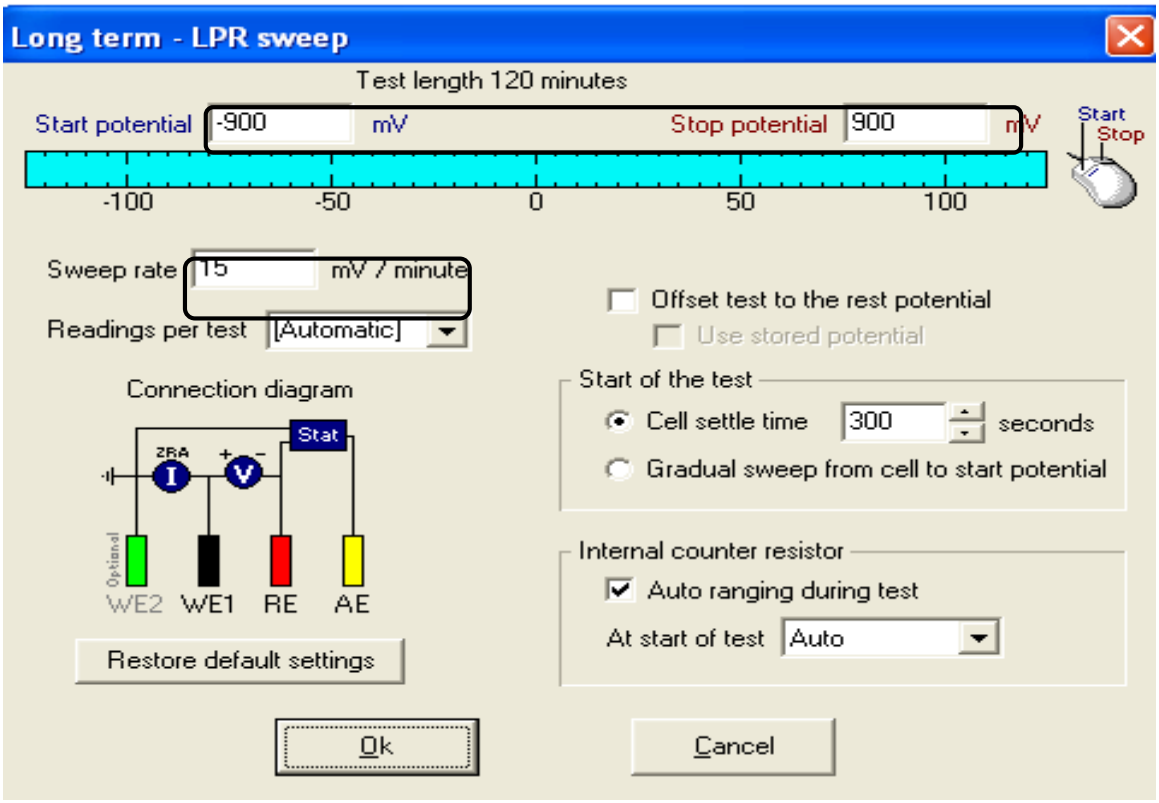

Figure 3.5: Potential Range and Scanning Rate as Appeared

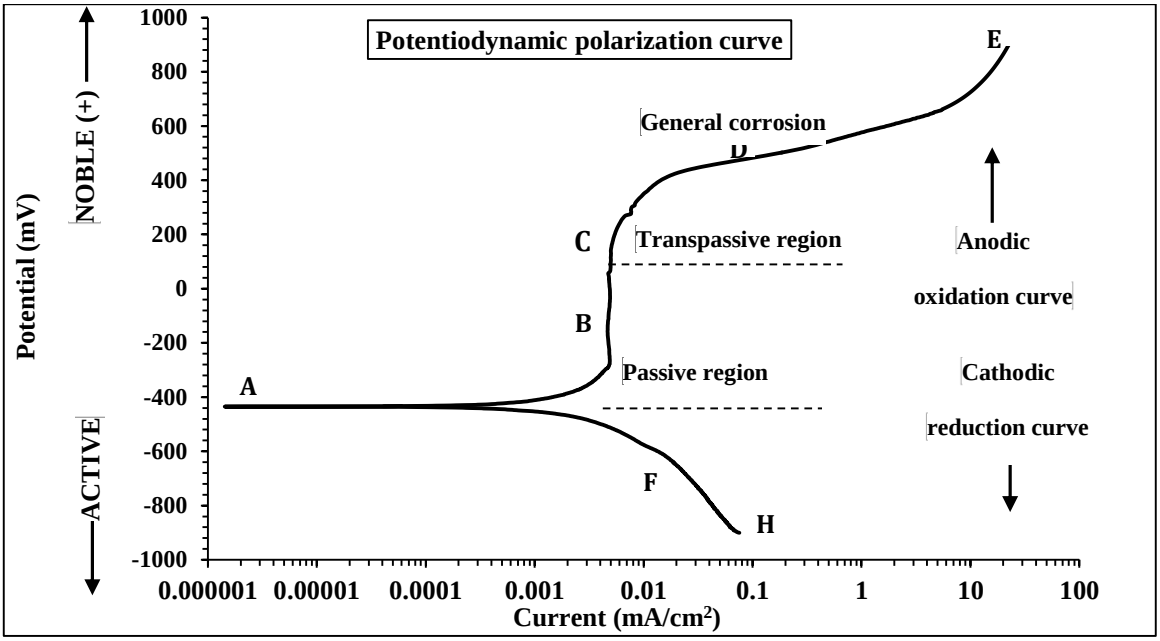

Figure 3.6: Schematic Illustration of Potentio-Dynamic Polarization with Various Terminologies

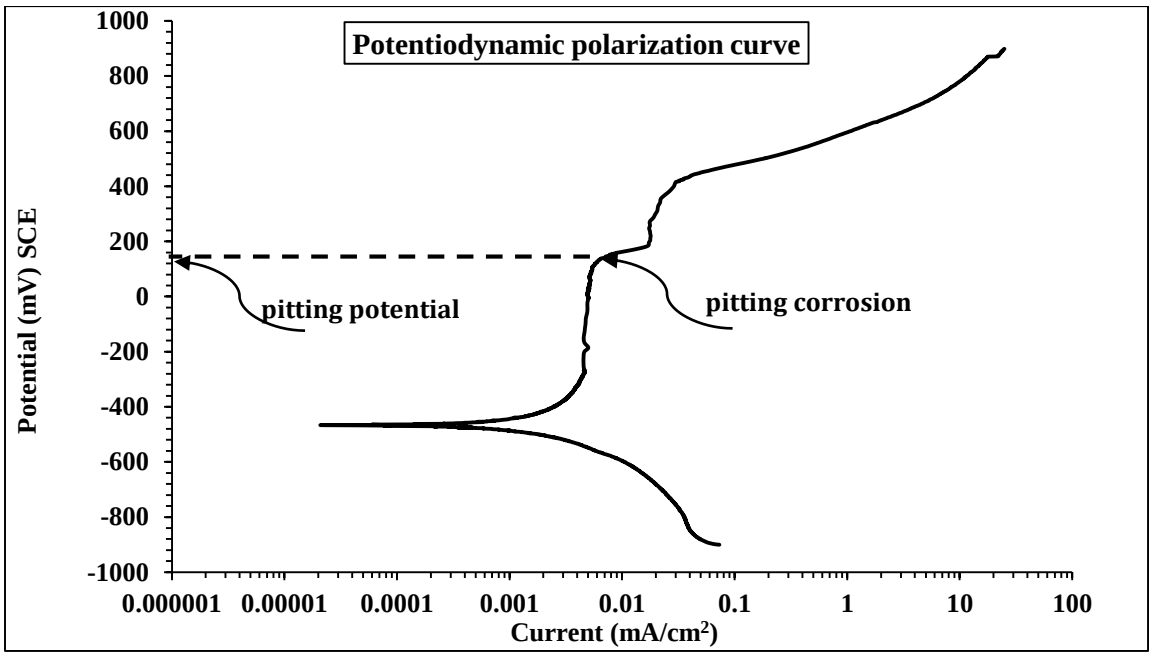

Figure 3.7: Schematic Illustration of Potentio-Dynamic Polarization with Pitting Corrosion

Significant information can be obtained from the potentio-dynamic polarization scan, some of which include the following:

i. The potential area over which the metal remains in passive stage.
ii. The corrosion rate of the metal sample in the passive area and the ability of the metal sample to be passivated.
iii. The localized corrosion of metal samples.

Passivity condition

3.2.5 Corrosion Current Density

For this test, ACM instrument with three electrodes was used to conduct the potentio-dynamic scan. The steel specimen with 28 mm length and 16 mm diameter, as described in Section 3.2.1, was connected to the working electrode terminal while reference electrode and small steel plate were connected to the respective terminals of the potentiostat. This specimen was polarized by applying a potential of ±900 mV of the corrosion potential with scan rate of 15 mV/minute and the resulting current between the working and counter electrodes is measured. Figure 3.8 shows a schematic representation of the set-up which was used to measure the corrosion current density. Also, Figure 3.9 shows general view of the experimental setup of corrosion current density test.

Figure 3.10 depicted the main terminologies in a polarization diagram which is plotted between the applied potential and log measured current. The solid lines represent cathodic and anodic reactions, whereas the dashed lines represent the linear part of each reaction. The

intersection of these dashed lines gives the open circuit potential (E_{corr}) on the vertical excise and corrosion current density on the horizontal axis. The anodic polarization curve is predominant at positive direction (Nobel), while cathodic polarization curve is predominant at negative direction (active). Then, the corrosion current density can be calculated using the Stern-Geary formula [52]:

$I_{corr} = B/R_p$ ………………………………………………………………….. (3.1)

Where:

I_{corr} = corrosion current density (μA/cm^2);

R_p = polarization resistance, KOhms-cm^2;

$B = (\beta a*\beta c)/(2.3(\beta a+\beta c))$;

Where: βc and βa are the cathodic and anodic Tafel constants, respectively.

The Tafel constants can be determined either by polarizing the steel to ±250 mV of the corrosion potential or polarizing the steel to ±900 mV of the corrosion potential (potentio-dynamic). In case of the absence of sufficient data on tafel constants, "a value of 100 mV is to be used for steel in a highly resistant medium" [53]. A good correlation between the linear polarization technique and the weight loss determined by gravimetric methods was observed by Gonzalez et al [54] by using a B value of 52 mV in the passive state and 26 mV for steel in the active state. In our investigation, βc = βa = 120 mV was used throughout which corresponds to B = 26 mV. These values have been found to be useful in the corrosion experiments at KFUPM.

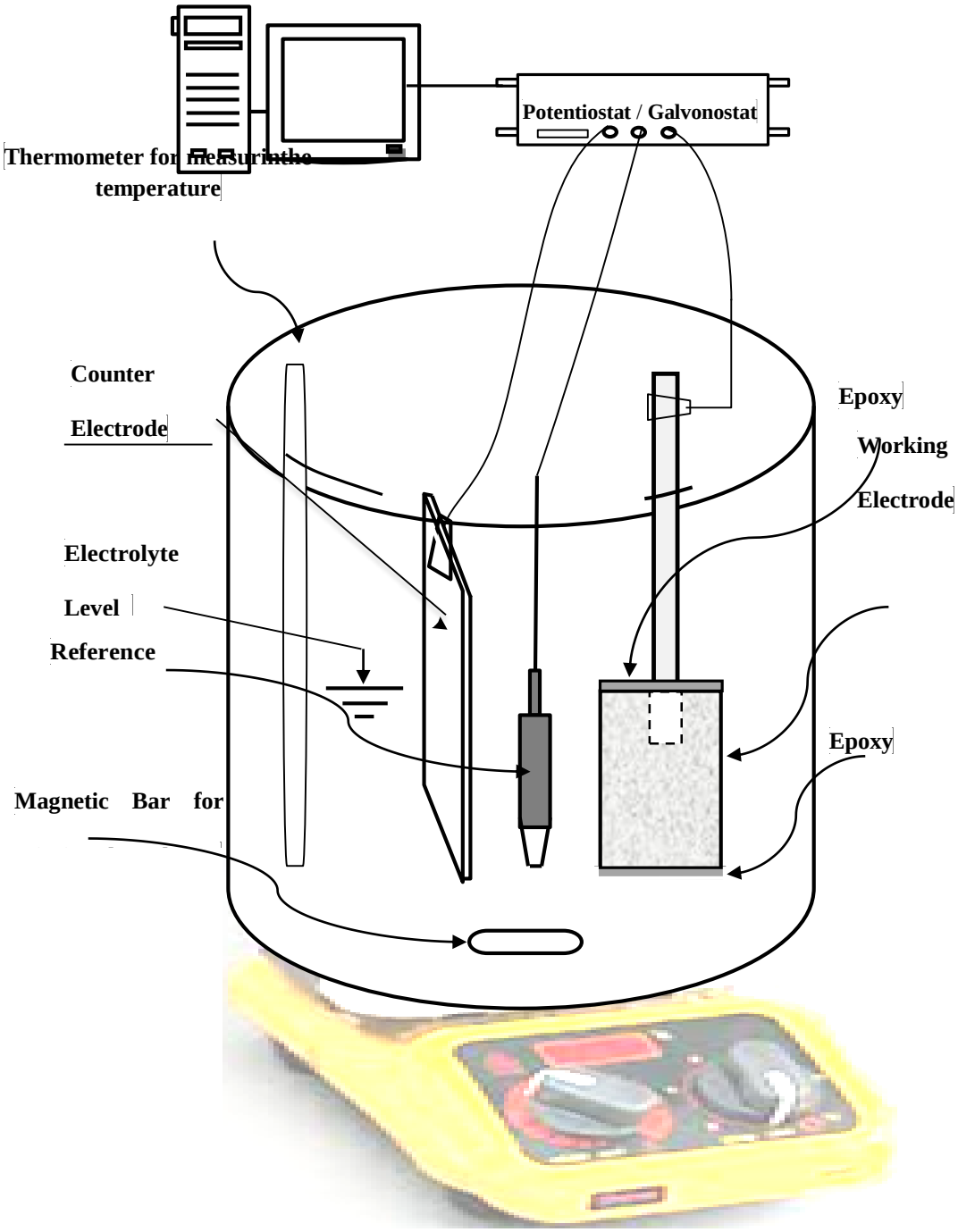

Figure 3.8: Schematic Representation of the Experimental Setup Used for Electro-Chemical Measurements

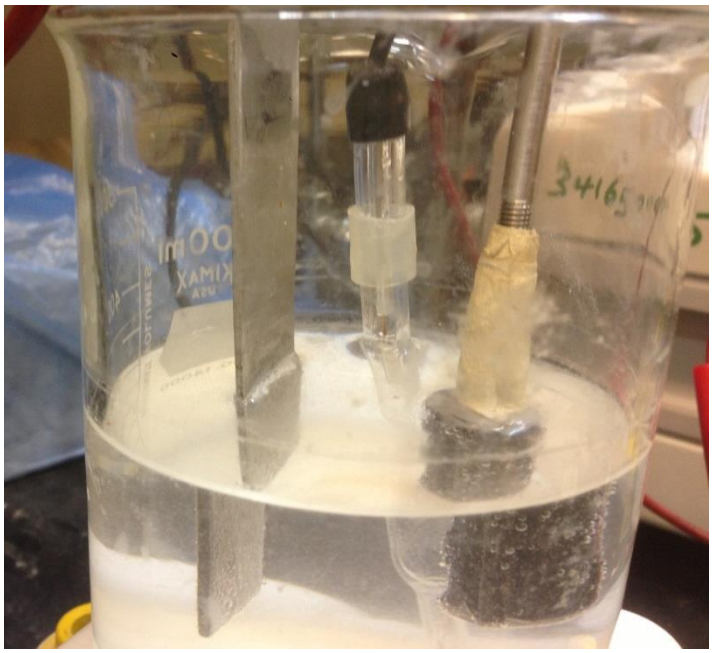

Figure 3.9: General View of the Experimental Setup for Electro-Chemical Measurements

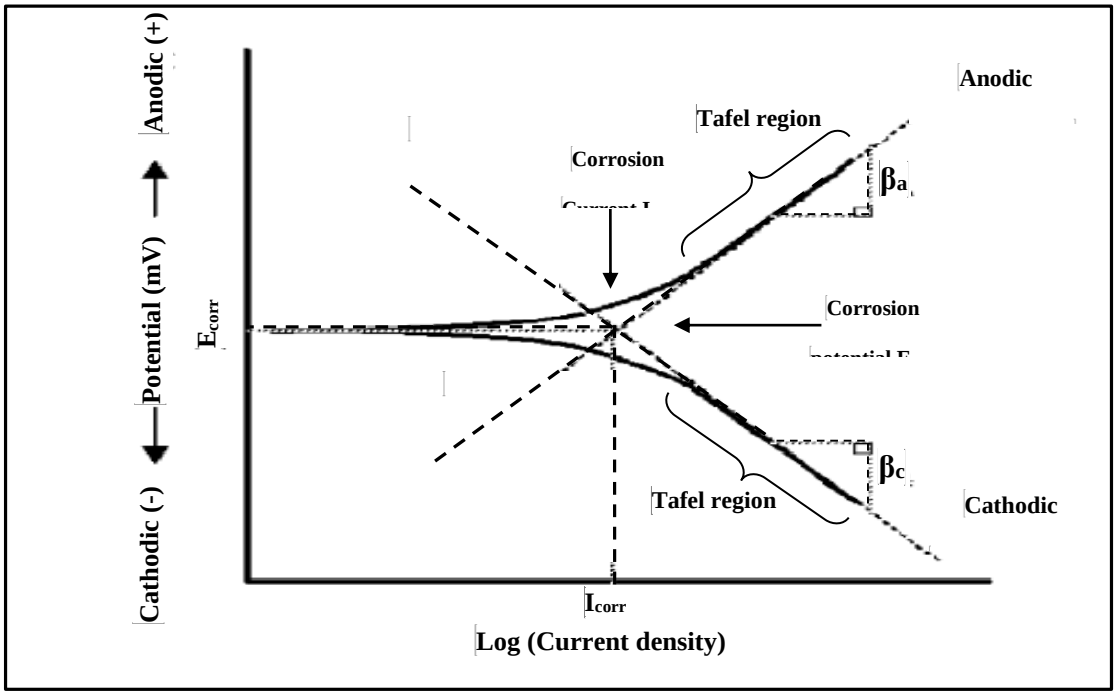

Figure 3.10: The Main Terminologies in Tafel Polarization Diagram

3.3 Scanning Electron Microscopy (SEM)

The scanning electron microscope (SEM) uses beam of high-energy electrons instead of light to generate variety of signals at the surface of solid samples. These signals reveal information about the sample including its chemical composition, external morphology (texture), and orientation of materials making up the sample, and crystalline structure. In this research, the surface of mild steel samples exposed to simulated concrete pore solution were evaluated using SEM to know the surface conditions. In order to conduct the proposed SEM test procedures, specialized equipment (Philips XL 30 SEM instrument) was used. The main components of this system includes: sample chamber, electron column, three visual display monitors and EDS detector, as shown in Figure 3.11.

Figure 3.11: Photographic Documentation of SEM Instrument showing the main Components

3.4 Metallography and Material Characterization

The steel rebar samples were prepared by grinding, polishing and etching in a 2 pct nital solution of as-received materials and heat-treated materials, As shown in Figure 3.12 . All Vickers hardness data were obtained along the cross section of the rebar samples. A 500 gmf and 200 gmf load were used for all hardness data. All micrographs taken for material characterization purposes were taken on the cross section sectioned of the rebar samples.

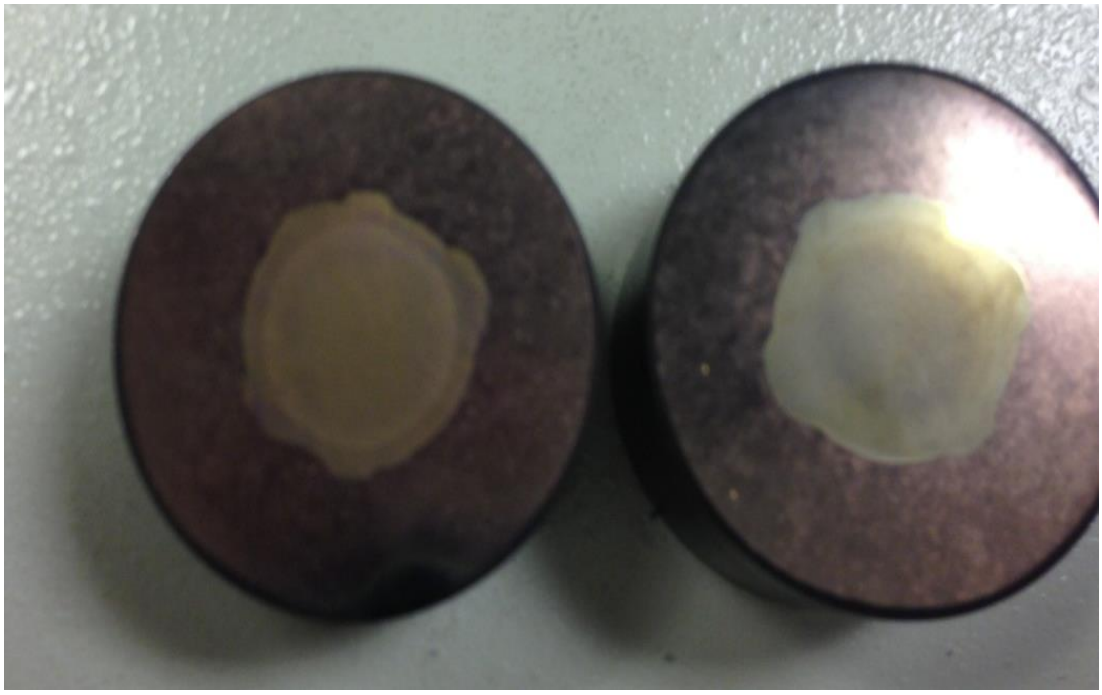

Figure 3.12: Steel rebar samples were prepared by grinding, polishing and etching for Metallography

3.5 Heat Treatment Procedure

The main objective of heat treatment is to simulate the microstructure of steel rebar to be use for corrosion tests. Heat treaTable samples were rough-machined from rebar samples as shown in Figure 3.13. These Samples were machined to this form to use it for heat treatment in the Gleeble. Gleeble 3500 Figure 3.14 were used to carry out the heat treatments with isothermally-transformed sets.

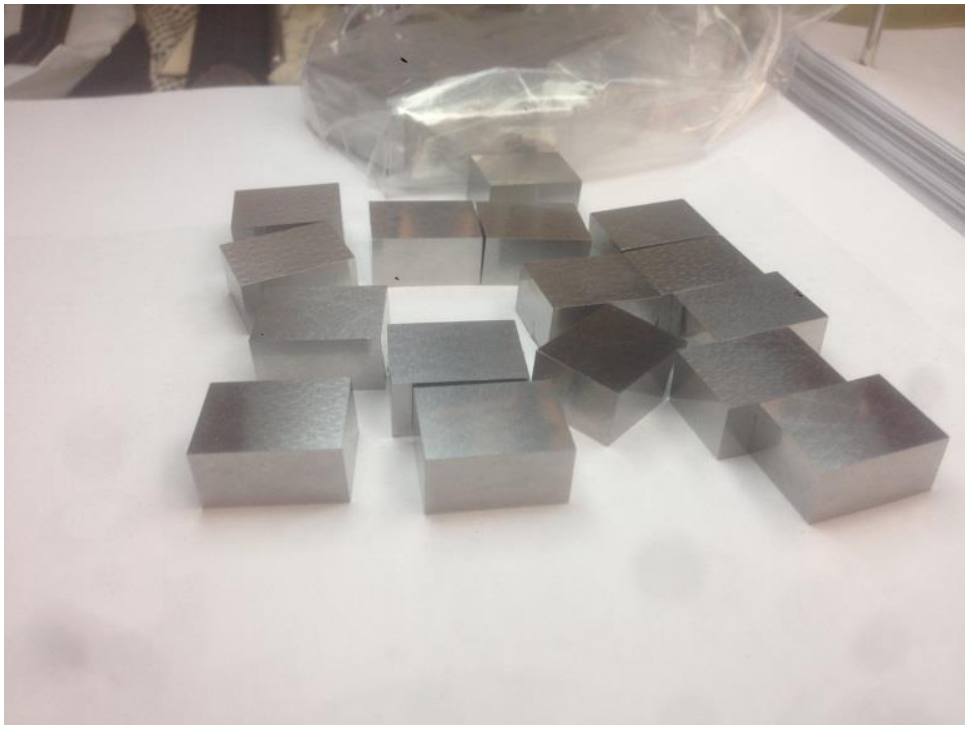

Figure 3.13: Rough-machined Rebar sample for heat treatment in the Gleeble.

3.5.1 Heat Treatment Schedules

From TTT Diagram four different microstructures namely tempered martinsite, bainite, fine pearlite and coarse pearlite were created. The heat treatment cycle by Gleeble is shown in the Table 3.2.

Table 3.2: Heat Treatment Schedules in the Gleeble.

Desired Microstructure	Procedure
Tempered Martinsite	Heat to 870 C for 1 minutes. Water quench. Heat to 400 C for 2 minutes Air cool.
Bainite	Heat to 870 C for 1minutes. Rapid cool to 450C and hold for 40 Sec. Air cool.
fine pearlite	Heat to 870 C for 1minutes. Rapid cool to 600C and hold for 100 Sec. Air cool.
coarse pearlite	Heat to 870 C for 1minutes. Furnace cool to room Temp.

CHAPTER 4

RESULTS AND DISCUSSION

This chapter presents the experimental results and discussions for this study. First, characterization of different steel rebar materials and comparing the corrosion resistance of the quenched steel rebar with air cooled steel rebar. Secondly, the results of simulated microstructures of steel rebar by various heat treatments and their corrosion resistances will be presented and discussed.

4.1 The Corrosion Resistance of Different Steel Rebar

Four samples used in this study were obtained from different companies. The results show that only one sample was produced by air cooling which is sample B, while the others were produced by water quenching. So, the comparison will be done between water quenching and air cooling samples.

4.1.1 Chemical Analysis by C/S & XRF Analyzer

Steel rebars were analyzed by using XRF technique to determine their elemental compositions. The samples were collected from the local Saudi market and analyzed using XRF and carbon silver analyzer as shown in Table 4.1. The carbon contents of sample A is 0.2876 %, sample B has 0.3659 %, sample C has 0.2802 % and sample D has 0.2701 %. It can be seen that Sample B has the highest carbon content which will improve its strength, while sample A has the lowest carbon content.

The chromium contents of sample A is 0.0986 %, sample B has 0.0529 %, sample C has 0.1653 % and sample D has 0.0351 %, from these values, it can be seen that Sample C has the highest chromium content.

Sample B has the highest manganese content of 1.2541% while sample D has the lowest manganese content. Sample A has the highest copper content of 0.2728% while sample C has the lowest manganese content.

Table 4.1: Chemical Analysis for rebar samples in Saudi Arabia.

	Sample A	Sample B	Sample c	Sample D
Elements	Conc.%	Conc. %	Conc. %	Conc. %
C	**0.2876**	**0.3659**	**0.2802**	**0.2701**
Al	0.0177	Tracing	0.0186	0.0116
Si	0.1795	0.2405	0.1795	0.1770
P	0.0381	0.0373	0.0351	0.0366
S	**0.0299**	**0.0293**	**0.0316**	**0.0223**
Ti	0.0047	0.0046	0.0050	0.0063
V	0.0050	0.0040	0.0120	0.0057
Cr	0.0986	0.0529	0.1653	0.0351
Mn	0.6566	1.2541	0.6775	0.6243
Fe	**Balance**	**Balance**	**Balance**	**Balance**
Ni	0.0912	0.0428	0.0746	0.0247
Cu	0.2728	0.1358	0.0972	0.1070
Nb	0.0037	0.0078	0.0190	0.0073
Mo	0.0183	0.0072	0.0375	0.0073

4.1.2 Metallography

The samples were cut from the cross section. Grinding and polishing were done according to standard “Preparation of Metallographic Specimens - ASTM E 3”. The samples were etched by using 2% Nital and examined under optical microscopy to identify the microstructure of the cross section as shown in Table 4.2.

Table 4.2 shows the macrostructure and microstructure of the rebars at the center and the outer surface for each sample. It can be seen a hardened layer appearing as show in sample A, C and D. On the other hand, there is no hardened rim appearing in Sample B.

It is clearly shown in Table 4.2 that Samples A, C and D have tempered martinsite microstructure in the outer surface layer that means cooled starting at the surface of the bar and the center is soft. At the transition from martensite to ferrite by quenching, while sample B has pearlite microstructure in outer surface layer due to cooling by air.

Table 4.2: Metallography Analysis of rebar etched by 2% Nital

	Macro photo	500x at Outer ring	500x at Inner ring
1.Sample A	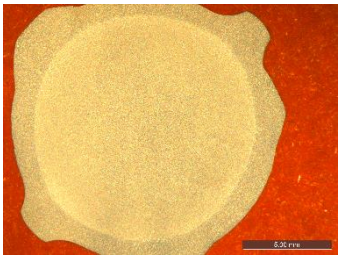	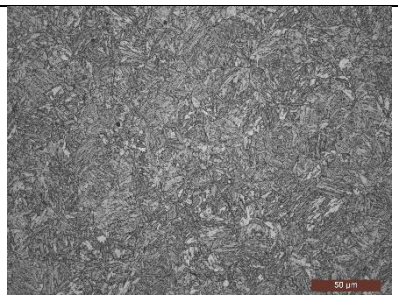	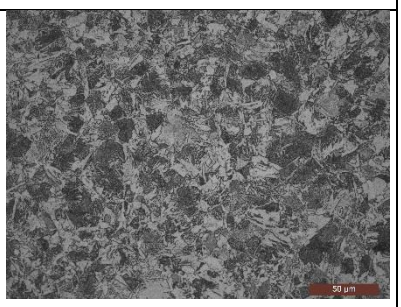
2. Sample B	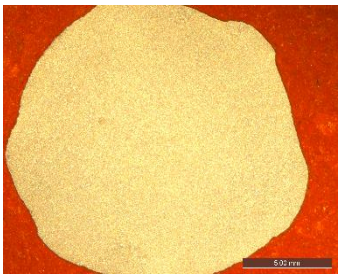	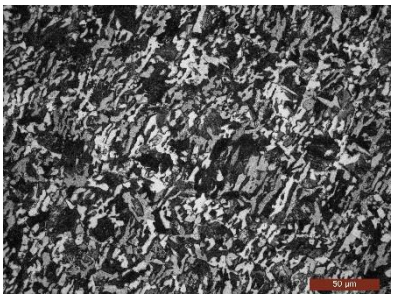	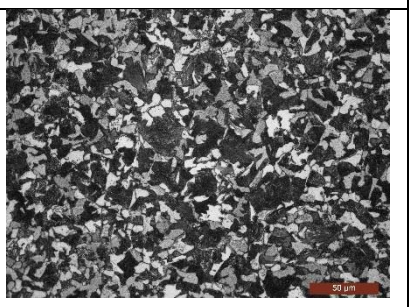
3. Sample C	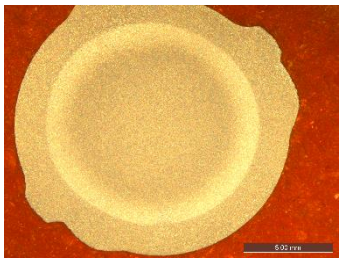	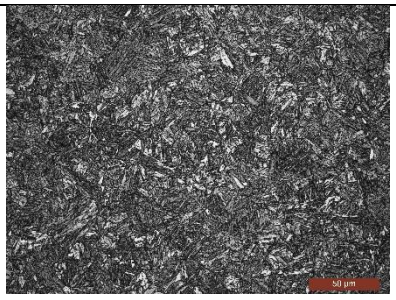	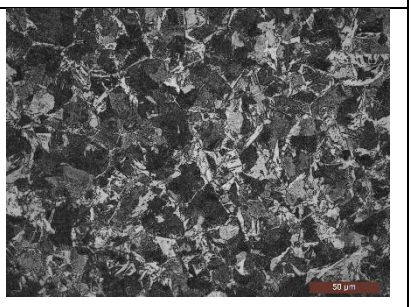
4. Sample D	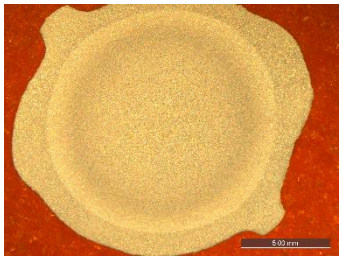	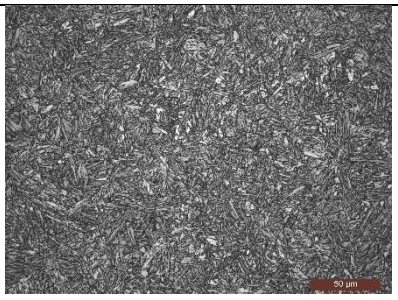	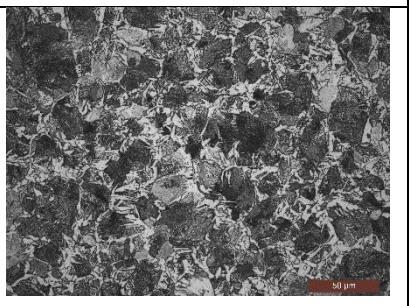

4.1.3 Hardness Test

Table 4.3 and Figure 4.2 show typical micro hardness measured for Samples A, B, C and D rebars. Test methods and procedures were conducted according to the following methods, preparation of metallographic specimens - ASTM E 3, Micro indentation Hardness of Materials - ASTM E384. Also, the load was 500Kg.

As shown in Table 4.3, It can be observed that sample A, C and D have hard layer in the outer surface with a value of 300 HV, while, sample B has uniform hardness along the cross section between 250HV and 200 HV.

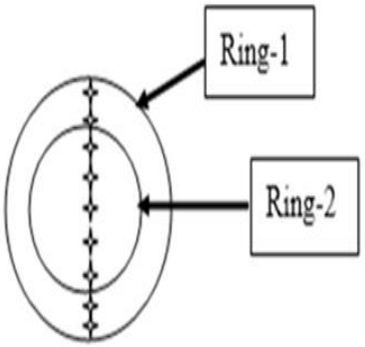

Figure 4.1: Location of typical microhardness indentation

Table 4.3: Micro indentation Hardness for Sample A, B, C and D.

Indentation NO	Sample A(HV)	Sample B(HV)	Sample C(HV)	Sample D(HV)
1	312.1	222.1	316.7	289.9
2	303.7	207.1	306.5	290.4
3	219.4	213.5	265	227
4	222.8	221.1	232.5	224.2
5	216.7	216.1	220.1	189.7
6	212.5	214.8	213.8	204.1
7	206.2	236.2	205.6	197
8	204.7	220.4	207.1	191.6
9	209	215.4	222.8	206.5
10	219	218.4	229.9	209.9
11	220.8	223.5	241.5	225.6
12	236.9	216.7	296.1	283.8
13	309	222	307.6	301

From Figure 4.2, shows the surface hardness of samples A, C and D and decreased from the surface to center as a result of quenching and tempering, while the hardness of sample B is almost uniform from the surface to the center due to the air cooling.

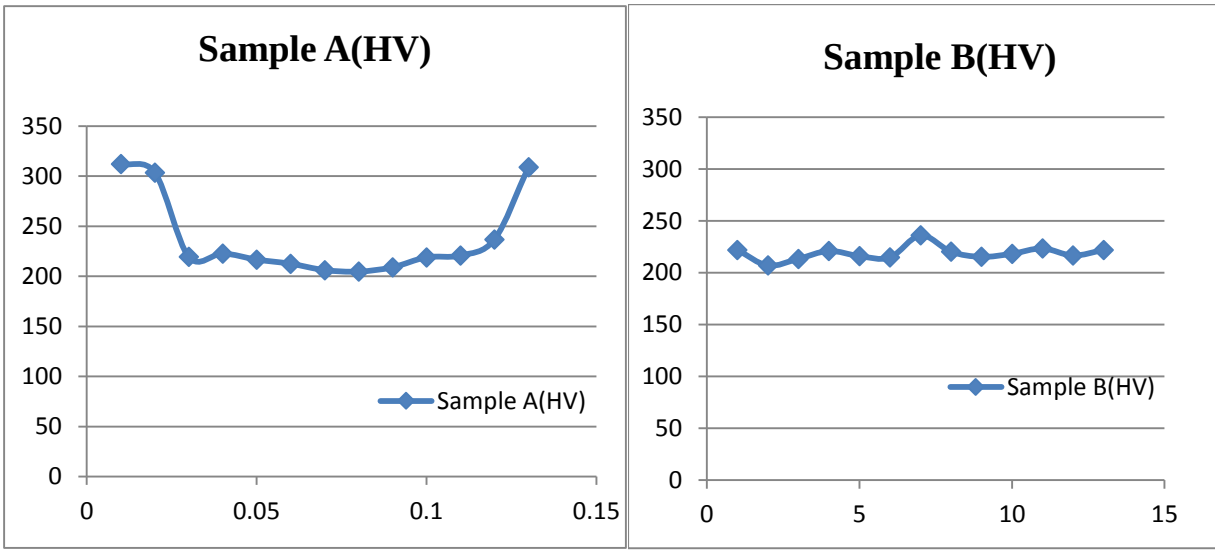

A) Hardness distribution Sample A

B) Hardness distribution Sample B

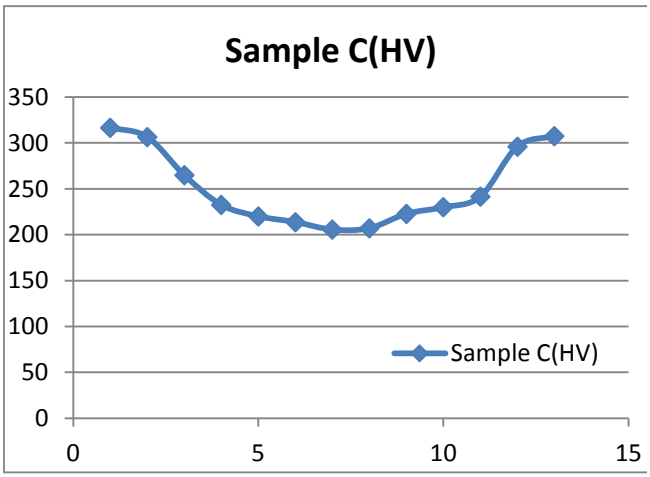

(C) Hardness distribution Sample C

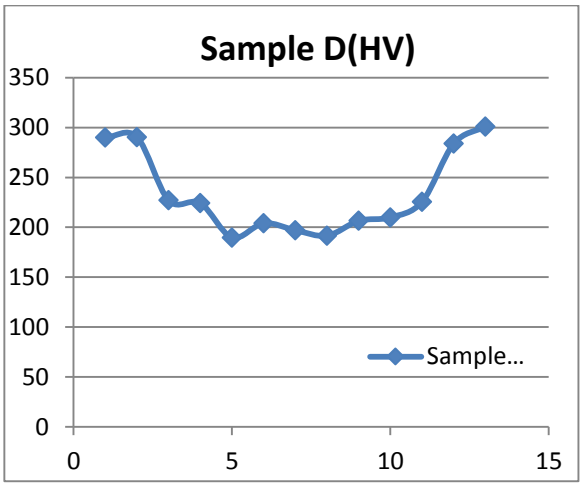

(D) Hardness distribution Sample D

Figure 4.2: Hardness distribution For (A) Sample A (B) Sample B (C) Sample C and (D) Sample D

4.1.4 Mechanical properties characterization

The tensile strength data were obtained from four specimens tested on a universal testing machine, and the yield strength, ultimate tensile strength (UTS) and elongation were determined for each condition. The diameters of the samples were 16 mm and Gauge lengths were 250 mm. And the test speed according to standard techniques were as following:

Rate 1: (To determine Yield properties): Strain rate to 0.015 mm/mm/min up to 2.0% of tensile strain. Rate 2: (To determine tensile properties): Strain rate to 0.402 mm/mm/min until complete fracture. The tensile tests were conducted at room temperature (23.3°C) on a 600kN Inston universal testing machine. Strain was calculated by 50 mm extensometer up to 2% strain. See Table 4.4 and Figure 4.3.

Table 4.4: Mechanical Properties of Rebars A, B, C and D

No.	Specimen Label	Proof Stress (Offset 0.2 %) (MPa)	UltimateTensile Strength (MPa)	Elongation-Auto (%)
1	Sample A-1	570	710	12.3
2	Sample A-2	570	710	11.9
3	Sample B-1	437	690	17.4
4	Sample B-2	441	700	18.4
5	Sample B-3	440	700	16.8
6	Sample C-1	610	705	11.8
7	Sample C-2	605	705	12.0
8	Sample C-3	605	695	9.8
9	SampleD-1	545	685	12.9
10	Sample D-2	545	680	13.7
11	Sample D-3	535	680	13.8

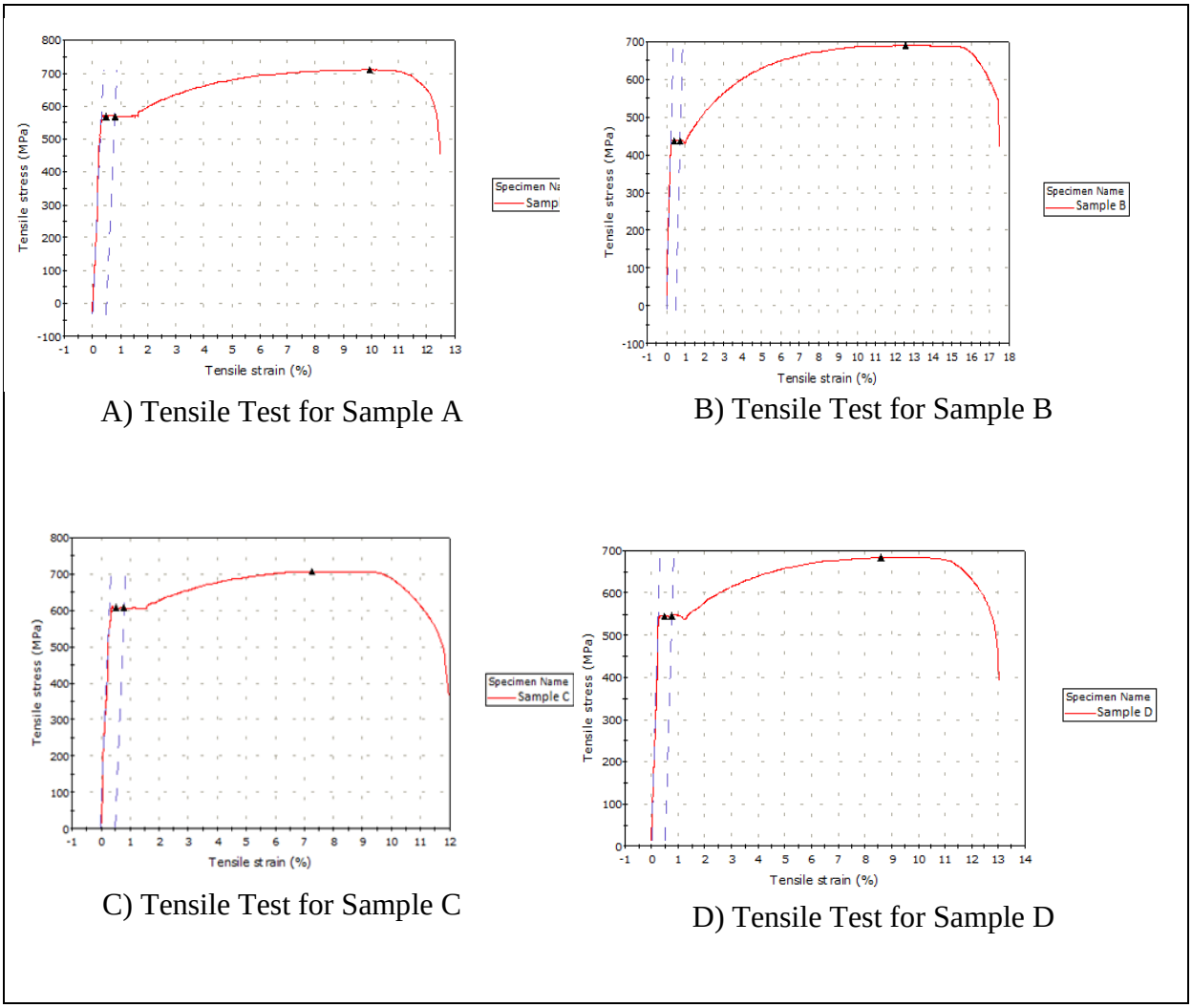

Figure 4.3: Stress-Strain Curves for Samples A, B, C and D.

4.1.5 Corrosion Test

The steel samples were prepared by cutting 28 mm length with 16 mm diameter, both ends of the specimen were coated with epoxy resin. Before the test, the specimens were degreased with acetone, rinse in distil water and dried in air. Potentiodynamic and linear polarization resistance studies were carried out on the exposed area of the bare steel exposed to electrolyte representing the concrete pore solution admixed with the selected chloride. The stimulated saturated concrete pore solution (SCPS) contains 10 g of NaOH, 14 g of KOH, 2 g of $Ca(OH)_2$ contaminated with sodium chloride ions concentration.

The potentiodynamic method measures the current for a large potential sweep from the cathodic to the anodic region of the corrosion potential. The potentiodynamic potential-current curves were generated by using the ACM potentiostat, scanning was done on the steel specimens using electrode potential from -900 to +900 mV with a scan rate of 15 mV/minute. Table 4.5 shows the result of the LPR tests, while the linear graphs are shown in Figure 4.4.

Table 4.5: Linear polarization resistance with 1000PPM of Cl^-

EXP NO.	BARS	Rest Potential (mV)	I_{corr} ($\mu A/cm^2$)	LPR value ($Ohm.cm^2$)	Corrosion rate (mm/year)
LPR	Sample A	-272.94	0.1899	137340	0.0022014
LPR	Sample B	-353.99	0.7007	37228	0.0081214
LPR	Sample C	-339.61	0.4520	57710	0.005239
LPR	Sample D	-458.37	0.6501	40127	0.0075348

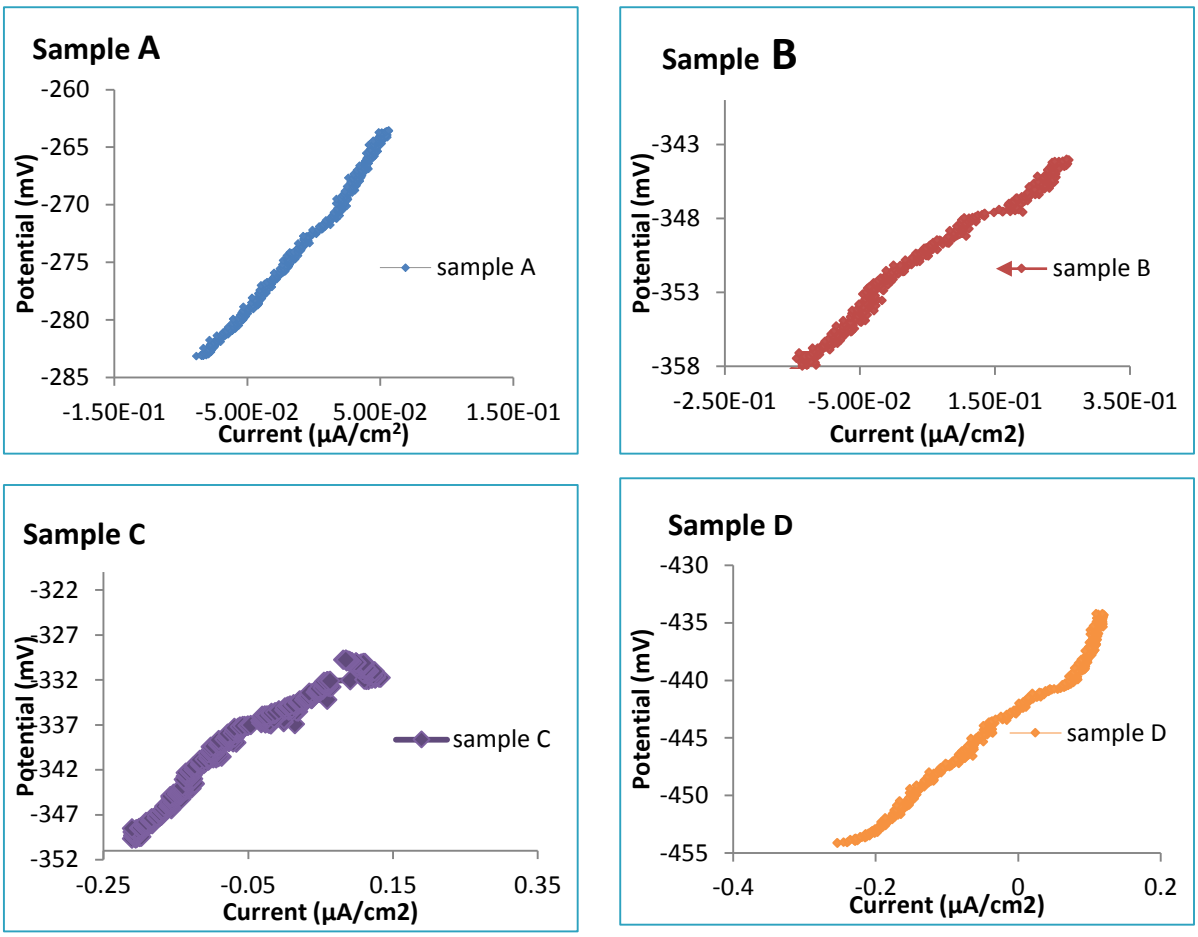

Figure 4.4: LPR graphs for the steel rebar.

Figure 4.5 depicts the corrosion current density (Icorr) on the selected steel bars exposed to saturated concrete pore solutions (SCPS) contaminated with 1000 ppm chloride ions. For the sample A, the Icorr was 0.1899 µA/cm^2, for the sample B, the Icorr was 0.7007 µA/cm^2, For the sample C, the Icorr was 0.452 µA/cm^2, while for sample D, the Icorr was 0.6501 µA/cm^2. This shows that the air cool sample has the highest Icorr while the quenched sample A has the lowest Icorr as shown in Figure 4.5. Also, figure 4.6 shows the Tefel curves for quenched sample A and the air cooled sample B.

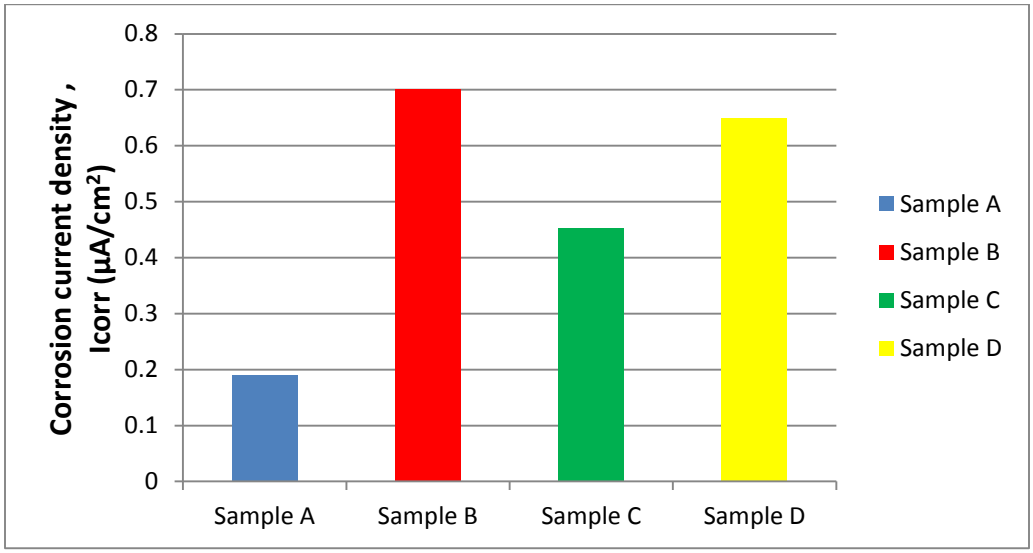

Figure 4.5: Bar Chart of LPR results.

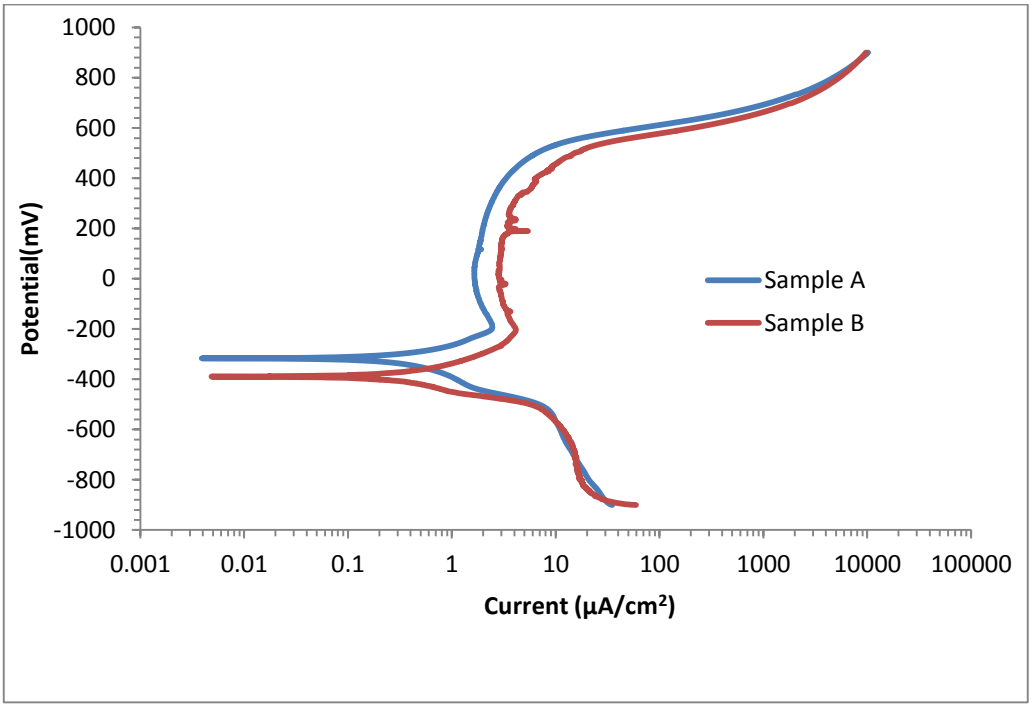

Figure 4.6: Potentiodynamic Tefel curves for sample A and Sample B steel bars immersed in pore solutions with 1000ppm CL^- .

Both curves show that the two specimens have approximately similar cathodic and anodic behaviour. However, the Tefel curve for sample B is slightly shifted to the right of smple A, indicating higher Icorr for air cooled sample B, than quenched sample A.

4.1.6 Scanning Electron Microscopy of Steel Specimens

Figure 4.7 depicts the scanning electron micrographs of the sample after polarization. General corrosion was observed on the specimens. The steel surface was rough and covered with corrosion products. All specimens showed no evidence of localized corrosion on the surface of the specimens tested.

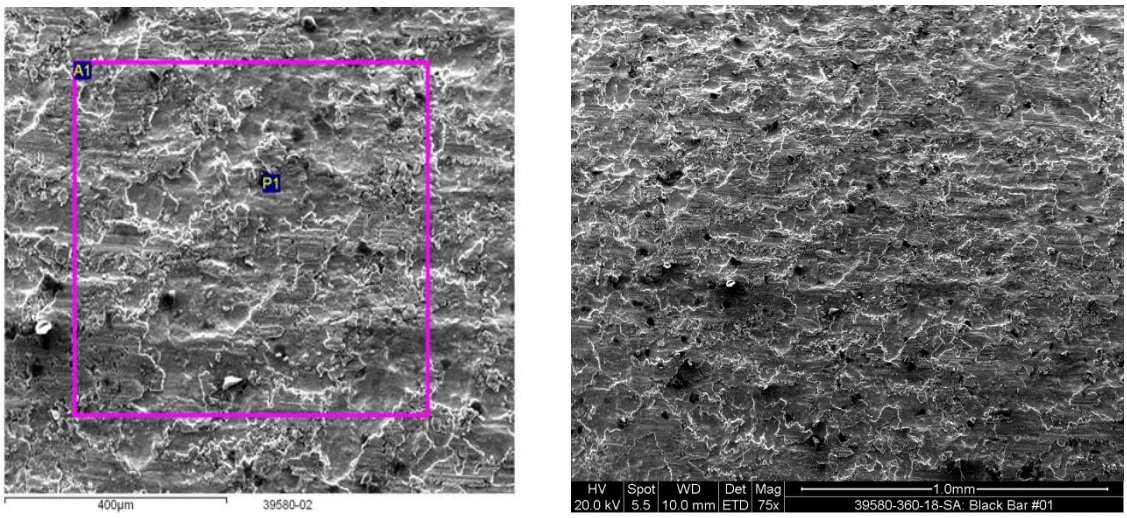

Figure 4.7: Close up Picture of SEM for Control Specimen with 1000 ppm Cl at 25 ºC.

The potentiodynamic and linear polarization resistance results revealed that an air cooled specimen B has the highest corrosion rate. While, other steel rebars have lower corrosion rates. Pearlite is a combination of two alternating phases, which are totally different in their electrochemical properties; the first phase is a carbon solid solution in iron with the bcc lattice, namely, ferrite (α iron) with a carbon concentration of no more than 0.02 wt % in an equilibrium state and 0.06 wt % in a non-equilibrium state [57], the second is iron carbide Fe_3C with the orthorhombic lattice, namely, cementite with a carbon concentration of 6.67 wt %. This difference leads to the formation of microgalvanic couples (electrochemical cells) with very different potentials, which promote gaivanic corrosion [58]. Since cementite in this structure is the phase most resistant to corrosion [59], the anodic dissolution of ferrite leads to the fact that the carbide phase that remains on the surface of the metal/medium interface increases the steel surface potential.

In Conclusion for section 4.1, the result of the corrosion resistance of Quenched steel rebar is higher than air cooling steel rebar. Also, as shown from the result of XRF, sample A has the highest amount of Cu. This might explain the reason for lowest corrosion rate of sample A.

4.2 Effect of Microstructure On The Corrosion Resistance Of Steel Rebar

This section presents the results of the simulated microstructure of steel rebar by heat treatment experimentation and its corrosion resistance. As shown in the previous section 4.1, Steel rebar quenched by water, such as sample A has three different layers or four different layers. So, in this section I will investigate these layers and the corrosion resistance of these layers.

4.2.1 As received Samples Hardness Test

. Steel rebar of 25 mm diameter was used in this study as shown in Table 4.6 and Figure 4.8. The typical micro hardness measured for the rebar sample along the cross section as shown in Figure 4.8. The tests samples were prepared according to the Preparation of Metallographic Specimens - ASTM E 3, The tests were conducted using micro indentation hardness of materials standard procedure - ASTM E384. The load used was 500 kg.

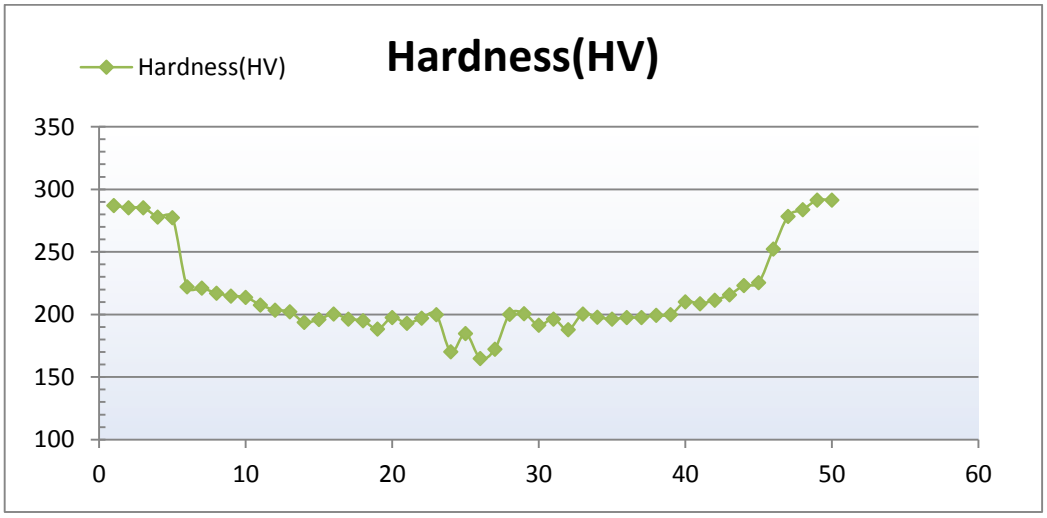

Figure 4.8: Hardness distribution along the cross section of steel rebar

Table 4.6: Hardness distribution along the cross section of steel rebar Size 25mm.

Indentation NO.	Hardness(HV)	indentation NO.	Hardness(HV)
1	287.2	**26**	165
2	285.3	**27**	172.3
3	285.3	**28**	200.2
4	278	**29**	200.8
5	277.5	**30**	191.4
6	222.1	**31**	196.4
7	221.1	**32**	187.8
8	217.1	**33**	200.5
9	214.8	**34**	197.8
10	213.8	**35**	196.4
11	207.7	**36**	197.6
12	203.5	**37**	197.6
13	202.3	**38**	199.3
14	193.9	**39**	199.9
15	196.1	**40**	210.2
16	200.5	**41**	208.7
17	196.4	**42**	211.5
18	195	**43**	215.7
19	188.4	**44**	223.2
20	197.6	**45**	225.6
21	193	**46**	252.4
22	197	**47**	278.4
23	199.9	**48**	283.8
24	170.2	**49**	291.4
25	184.9	**50**	291.4

4.2.2 As received sample metallography analyses

The samples were cut from the cross section. After that grinding and polishing were done according to standard "Preparation of Metallographic Specimens - ASTM E 3". The samples were etched by using 2% nital and displayed to optical microscopy to identify the microstructure of the cross section.

The microstructure of selective rebar samples have been investigated and the diameter of all samples were 25 mm, Figure 4.9 shows the macrostructures and microstructures of the rebar at the outer surface and the other layers. It can be seen that they have four different layers which are tempered martensite, bainite, fine perlite, and coarse pearlite.

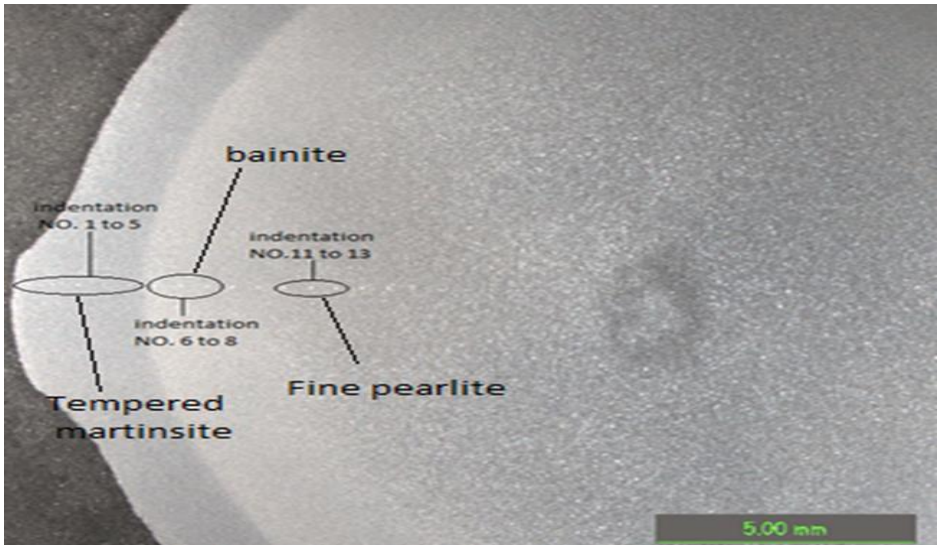

Figure 4.9: Macro photo for Steel Rebar size 25 mm

4.2.3 Microstructure of Steel rebar

Figure 4.10 to 4.13 show the microstructures of the heat treated steel samples. Figure 4.10 depicts the microstructure of tempered martensite which is extremely fine and uniform cementite in a continuous ferrite matrix. Also, tempered martensite is more rounded at the edges and appears more uniform structure than martensite, still sharp but not as coarse, while, untempered martensite appears coarse, sharp and harder.

Figure 4.11 depicts bainite as a plate-like microstructure or phase morphology (not an equilibrium phase). Also, it has a fine non-lamellar structure which consists of cementite and dislocation-rich ferrite. The high concentration of dislocations in the ferrite present in bainite. Cementite is shown like discontinuous "stringers" or laths. So, Bainite consists of very fine and parallel needle-shaped particles of cementite that are surrounded by α-ferrite matrix.

Figure 4.12 depicts the fine pearlite microstructure which is a lamellar (layered or plate-like) structure composed of alternating layers of ferrite and cementite. Also, fine pearlite is harder and stronger than coarse pearlite because there is more phase boundary area.

Figure 4.13 depicts coarse pearlite microstructure which is a lamellar structure composed of alternating layers of ferrite and cementite.

Tempered martinsite 500X

Tempered martinsite 200X

Figure 4.10: Microstructure of steel rebar tempered martinsite layer

Bainite 500X

Bainite 200X

Figure 4.11: Microstructure of steel rebar bainite layer.

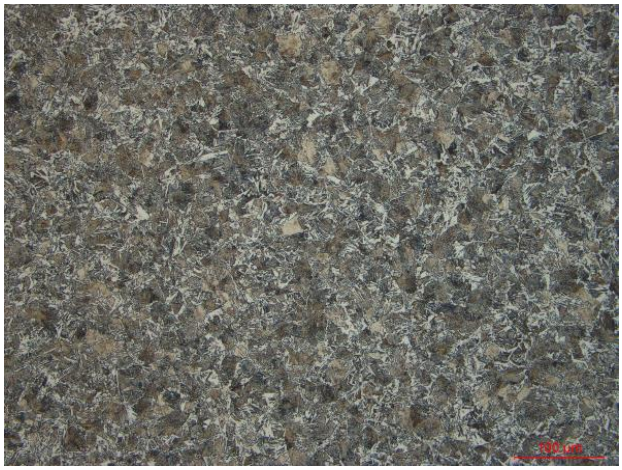

Fine pearlite 200X

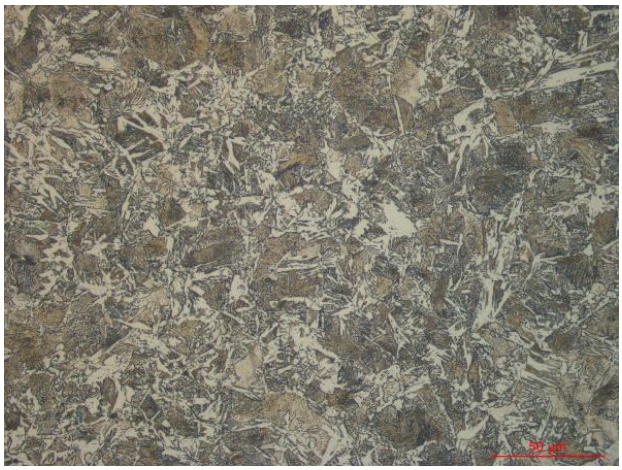

Fine pearlite 500X

Figure 4.12: Microstructure of steel rebar fine pearlite layer.

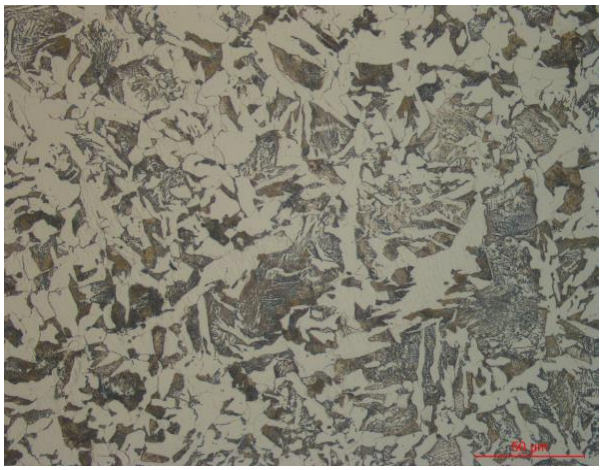

coarse pearlite 500X

Figure 4.13: Microstructure of steel rebar coarse pearlite layer.

4.2.4 Heat treatment samples

This section will present the result of heat treatment cycle done by Gleeble on each sample to produce the required microstructure and will show the hardness result and Metallography Analyses for each heat treatment cycle.

4.2.5 Tempered martensite

The steel specimens are heated to a temperature 870 °C at holding time of 1 min by gleeble furnace. Then cooled rapidly (quenching) by water nozzles inside the gleeble furnace to room temperature. Carbon steel quenched from these temperatures has a structure called martensite. The speed of quenching can affect the amount of marteniste formed. Martensite plates are hard and brittle that its need to be modified for practical applications. To stabilize the structure, alleviate the brittleness and develop useful mechanical properties, quenching is always followed by tempering. This process allows carbon atoms to diffuse out of the distorted lattice structure associated with martensite, and thus relieve some of the internal stresses. In this study, tempering is done by heating the specimens to a temperature 400 C° for 2 minutes and air cooling as shown in Figure 14. Tempering process results in the formation of tempered martensite and the hardness of tempered martesite is shown in Table 4.7.

Microstructure of TM heat Treatment cycle

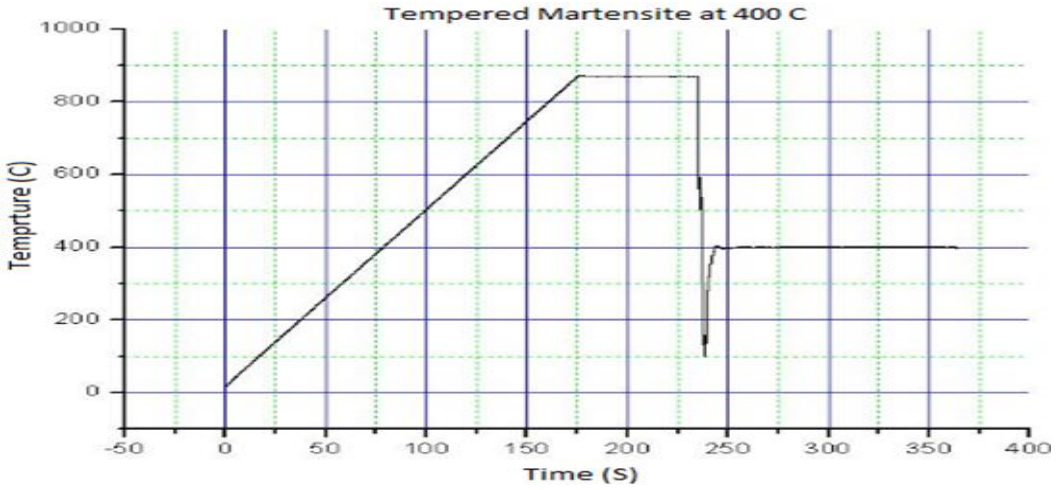

Figure 4.14: Heat treatment cycle for tempered martensite.

Table 4.7: **Hardness of Tempered Martensite heat Treatment cycle.**

Indentation NO.	**Hardness(HV)**
1	278
2	286
3	280
Average	281

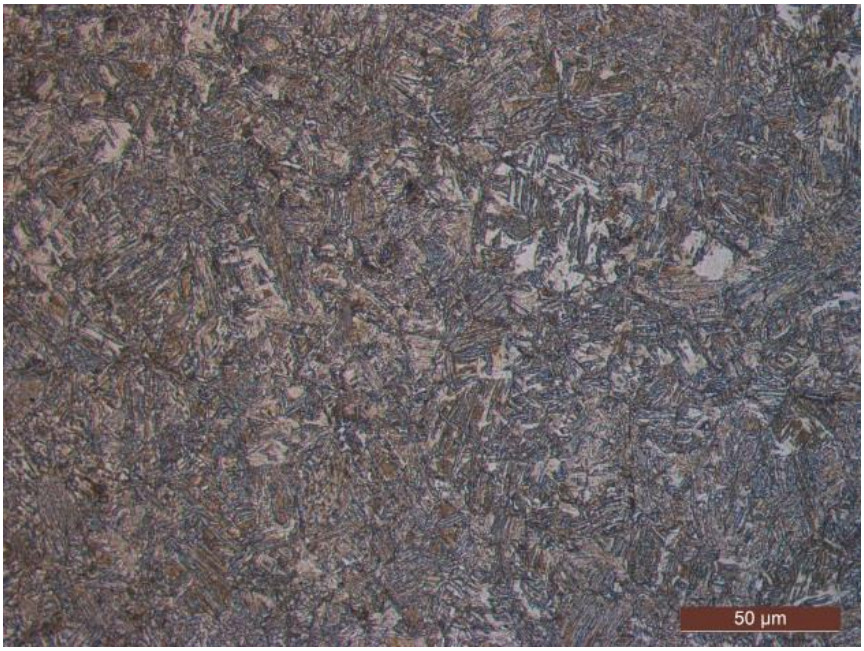

Figure 4.15: Microstructure of Steel rebar TM heat Treatment cycle 500x

4.2.6 Bainite microstructure

The steel specimens were heated to a temperature 870 °C at holding time of 1 min by gleeble furnace. Then cooled rapidly to 450 °C and hold for 40 seconds as shown in Figure 4.16, after that, they were air cooled.

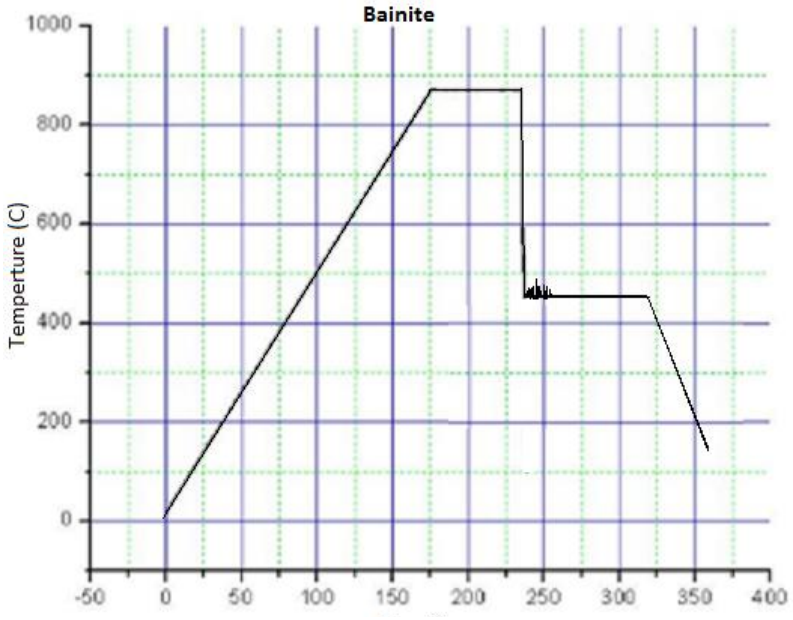

Figure 4.16: Heat treatment cycle for Bainite.

Table 4.8:Hardness of Bainite heat treatment cycle

Indentation	**Hardness**
1	224
2	219
3	223
Average	222

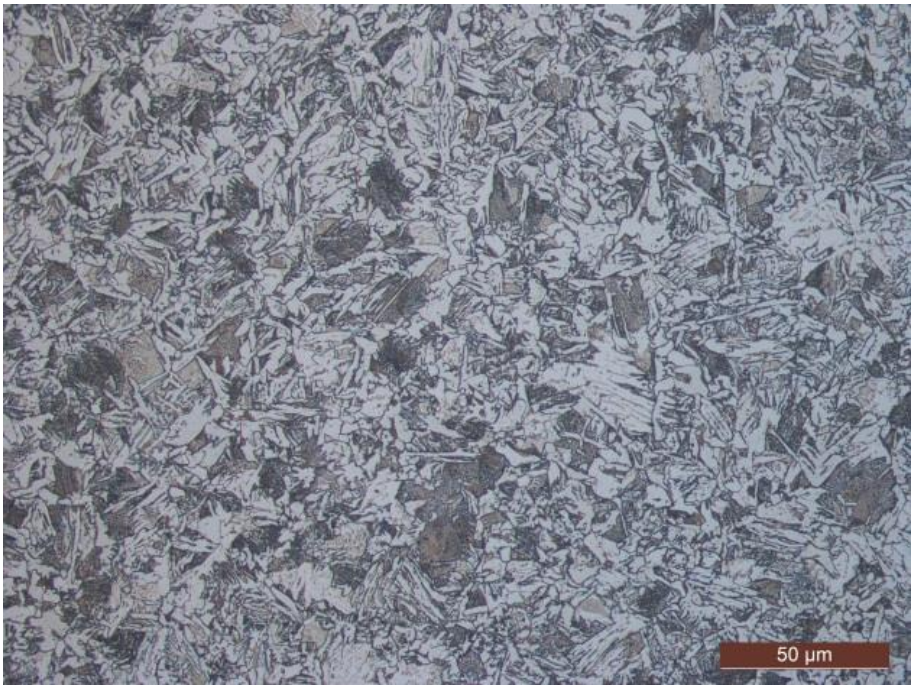

Figure 4.17: Microstructure of Steel rebar Bainite heat Treatment cycle 500x.

4.2.7 Fine pearlite

The steel specimens are heated to a temperature of 870 °C at holding time of 1 min by gleeble furnace. Then cooled rapidly to 600 °C and held for 100 Seconds, then air cooled.as shown in Figure 4.18. Finer pearlite need to be cooled down faster than coarse pearlite. The microstructure of fine pearlite is depicted in Figure 4.19. Also, the hardness value of fine pearlite is between the hardness of bainite and coarse pearlite as shown in Table 4.9.

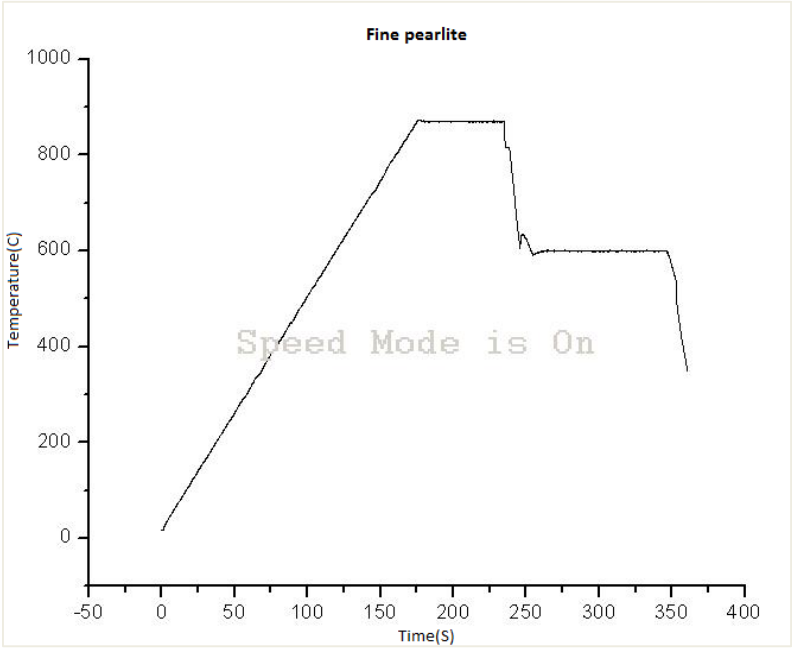

Figure 4.18: Heat treatment cycle for fine pearlite.

Table 4.9: Hardness of fine pearlite heat Treatment cycle**.**

Indentation No	**Hardness (HV)**
1	206
2	204
3	205
Average	205

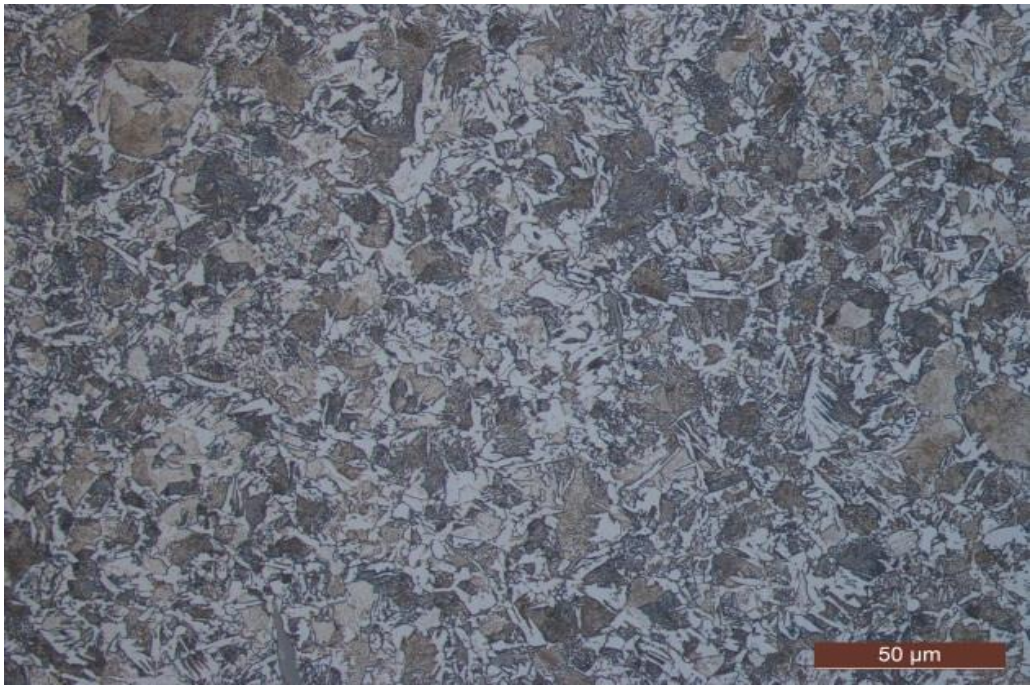

Figure 4.19: Microstructure of Steel rebar fine pearlite heat Treatment cycle 500X.

4.2.8 Coarse pearlite

The steel specimens are heated to a temperature of 870 °C at holding time of 1 min. Then, normal cooled inside gleeble furnace as shown in Figure 4.20. Coarse pearlite for which the alternating ferrite and cementite layers are relatively thicker than fine pearlite as shown in Figure 4.21. Also coarse pearlite has the lowest hardness value as shown in Table 4.10.

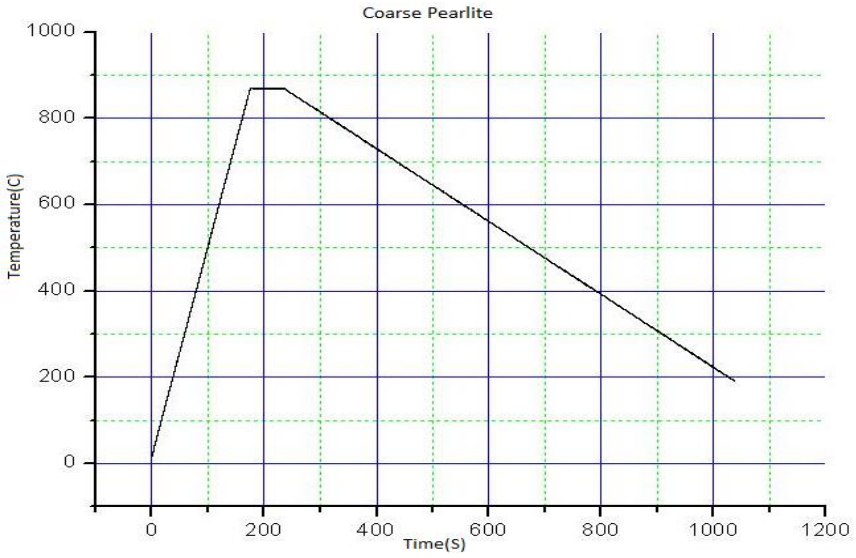

Figure 4.20: Heat treatment cycle for coarse pearlite normal cooling.

Table 4.10: Hardness of coarse pearlite heat Treatment cycle.

Indentation No	**Hardness (HV)**
1	196
2	188
3	187
Average	187

Figure 4.21: Microstructure of Steel rebar coarse pearlite heat Treatment cycle 500x.

4.3 Comparison of hardness and microstructures of as received rebar and heat treated samples

Figure 4.22 and Table 4.11 show the comparison of hardness of as received sample and heat treated samples. It shows the hardness range of tempered martensite (287 HV to 278HV), bainite (222 HV to 217 HV), fine pearlite (207 HV to 202 HV), and coarse pearlite (190 HV to 195 HV). The hardness values of heat treated samples are similar to the hardness range of as received sample for tempered martensite, bainite, fine pearlite and course pearlite range.

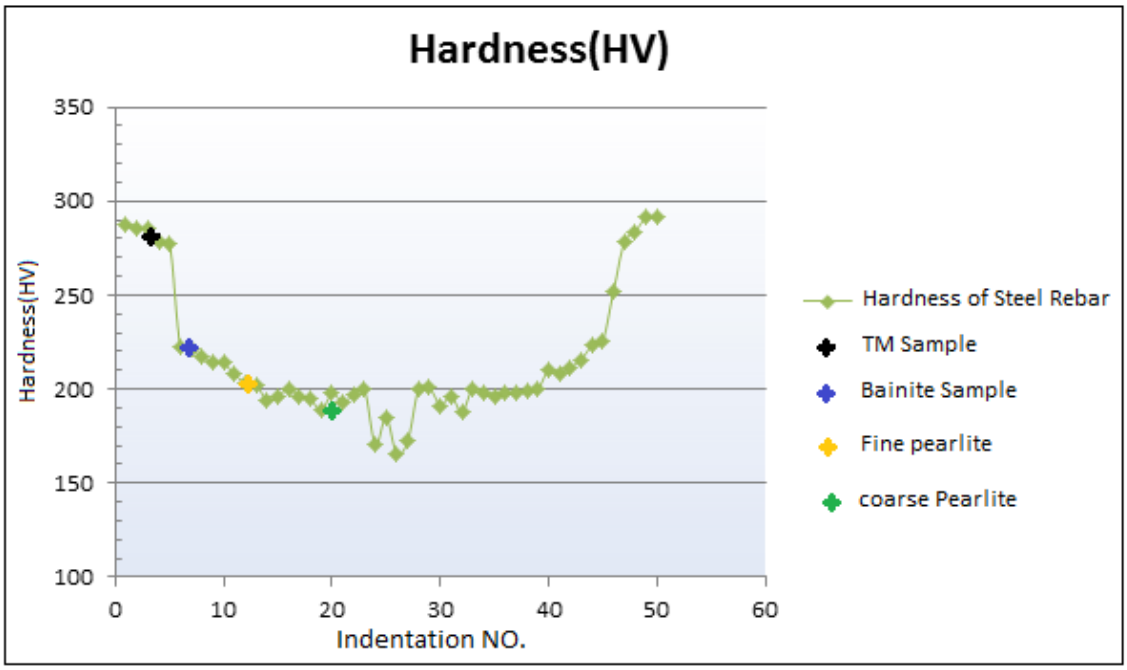

Figure 4.22: Comparison of hardness for as received sample with heat treated samples.

Table 4.11: Average hardness of Steel Rebar and Average hardness of single phase Sample.

Microstructure	Average hardness of Steel Rebar	Average hardness Single phase Sample
Tempered Martensite	283	281
Bainite	221	221
Fine Pearlite	205	205
Coarse Pearlite	193	190

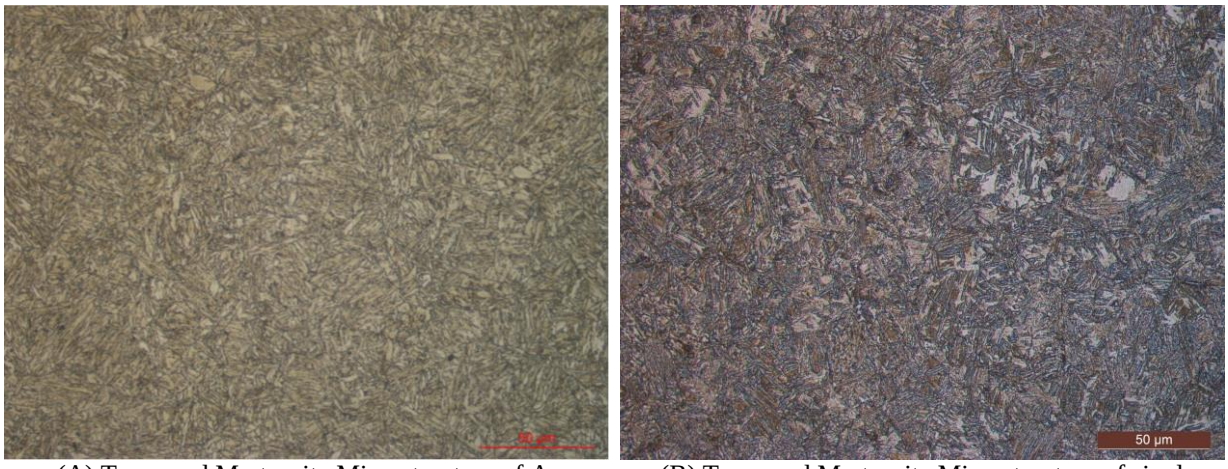

(A) Tempered Martensite Microstructure of As received Steel Rebar sample

(B) Tempered Martensite Microstructure of single phase Sample

Figure 4.23: Comparison of microstructures for tempered martensite (a) as received sample (b) heat treated sample

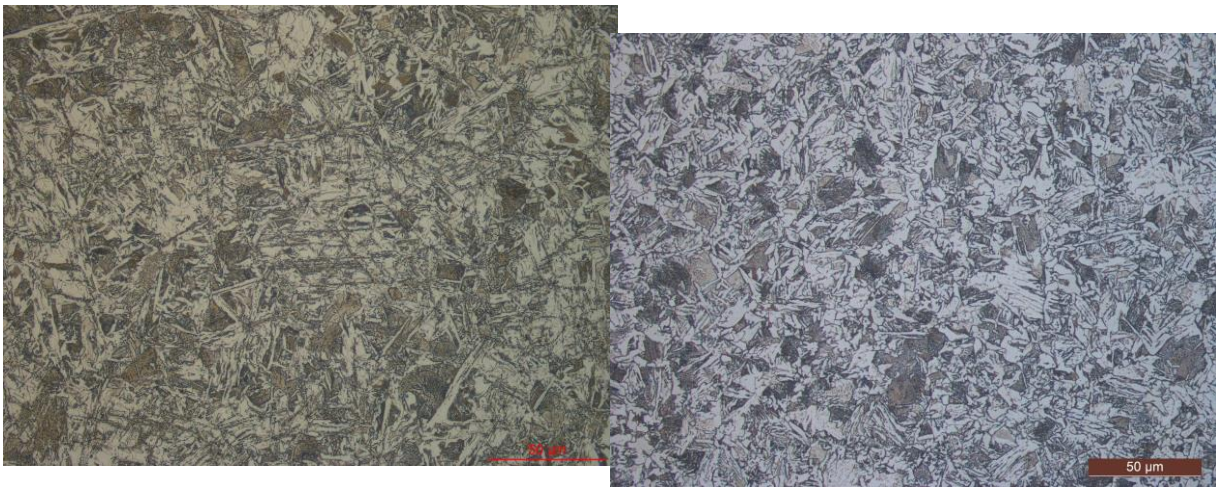

A) Bainite Microstructure of Steel Rebar

B) Bainite Microstructure of single phase Sample

Figure 4.24: Comparison of Microstructures for Bainite (a) As received sample (b) heat treated sample

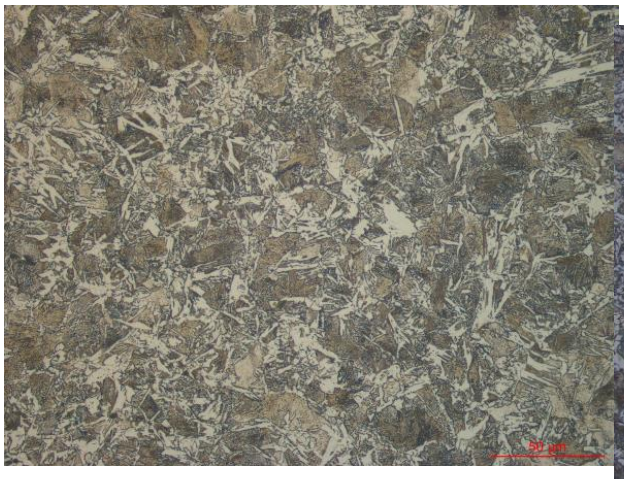

A) Fine Pearlite Microstructure of Steel Rebar sample

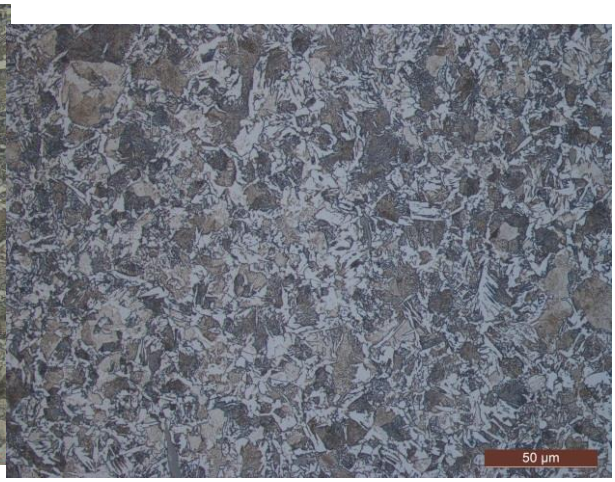

A) Fine Pearlite Microstructure single phase Sample.

Figure 4.25: Comparison of Microstructures for Fine Pearlite (a) As received sample (b) Heat treated sample.

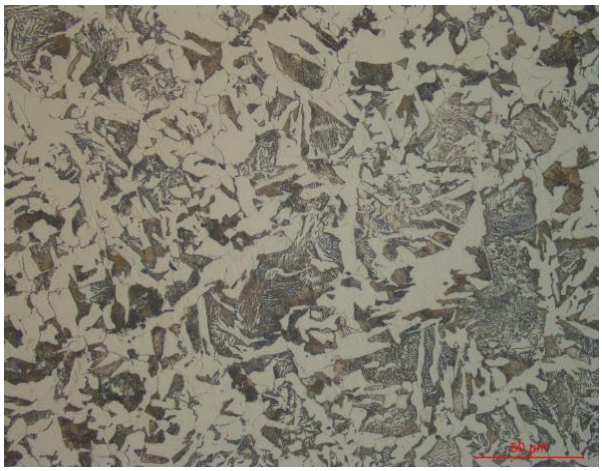

(A) Coarse Microstructure of Steel Rebar sample

(B)Coarse Pearlite Microstructure single phase Sample.

Figure 4.26: Comparison of Microstructures for coarse Pearlite (a) As received sample (b) heat treated sample.

As shown in Figure 4.25 and Figure 4.26, the hardness and microstructure of heat treated samples by gleeble (single phase) are comparable to as received rebar sample. Thus, the single phase samples can be used in the next section to study the corrosion resistance for each microstructure.

4.4 Corrosion Test for Single Phase Samples

4.4.1 Electrochemical impedance spectroscopy (EIS)

The corrosion response of heat treated steel specimens in 3.5% NaCl solution has been investigated using electrochemical impedance spectroscopy at room temperature, and Nyquist plots are represented in Figure 4.27.

The arc represents the combined effects of Rs (the solution resistance) Qdl (the capacitance of electrical double layer) and Rct (the charge transfer resistance). The results can be interpreted in terms of the equivalent circuit models in the electrical double layer Rs(QdlRct) [60] , as shown in Table 4.12.

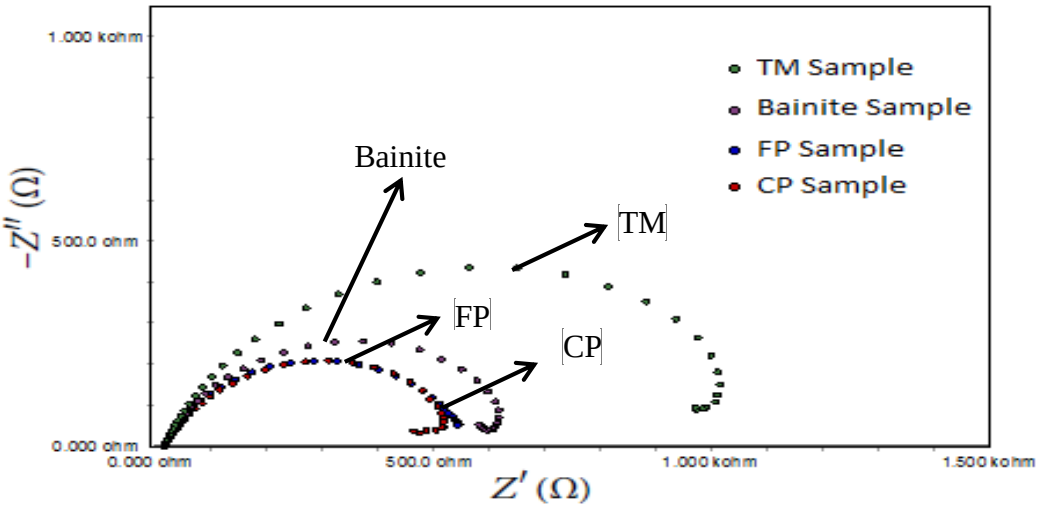

Figure 4.27: EIS curves (Nyquist) for heat treated steel samples in 3.5% NaCl

Table 4.12: Electrochemical impedance parameters of heat treated steel samples in 3.5% NaCl at room temperature

	R_S Ω	C or Qdl(F/cm^2)	N	R_{CT} Ohm
Tempered Martensite	17.67	5.26E-04	8.07E-01	1.08E+03
Bainite	16.95	5.38E-04	8.04E-01	631
Fine Pearlite	18.37	8.05E-04	7.85E-01	526.6
Coarse Pearlite	17.23	9.30E-04	7.92E-01	557.6

4.4.2 Linear Polarization Resistance (LPR) and Potentiodynamic polarization PDP Tests

Figure 4.28 shows the LPR graphs for the heat treated samples. Figure 4.38 shows the polarization curves for heat treated steel Samples (Tempered martensite , Bainite, Fine perlite, and coarse pearlite) in 3.5% NaCl at room temperature. All the examples exhibit uniform corrosion without any sign of pitting corrosion.

Table 4.13 depicts the corrosion current density (I_{corr}) on the heat treated samples exposed to 3.5 % NaCl using LPR. This shows that the TM has the highest corrosion resistance while the fine pearlite has the least corrosion resistance.

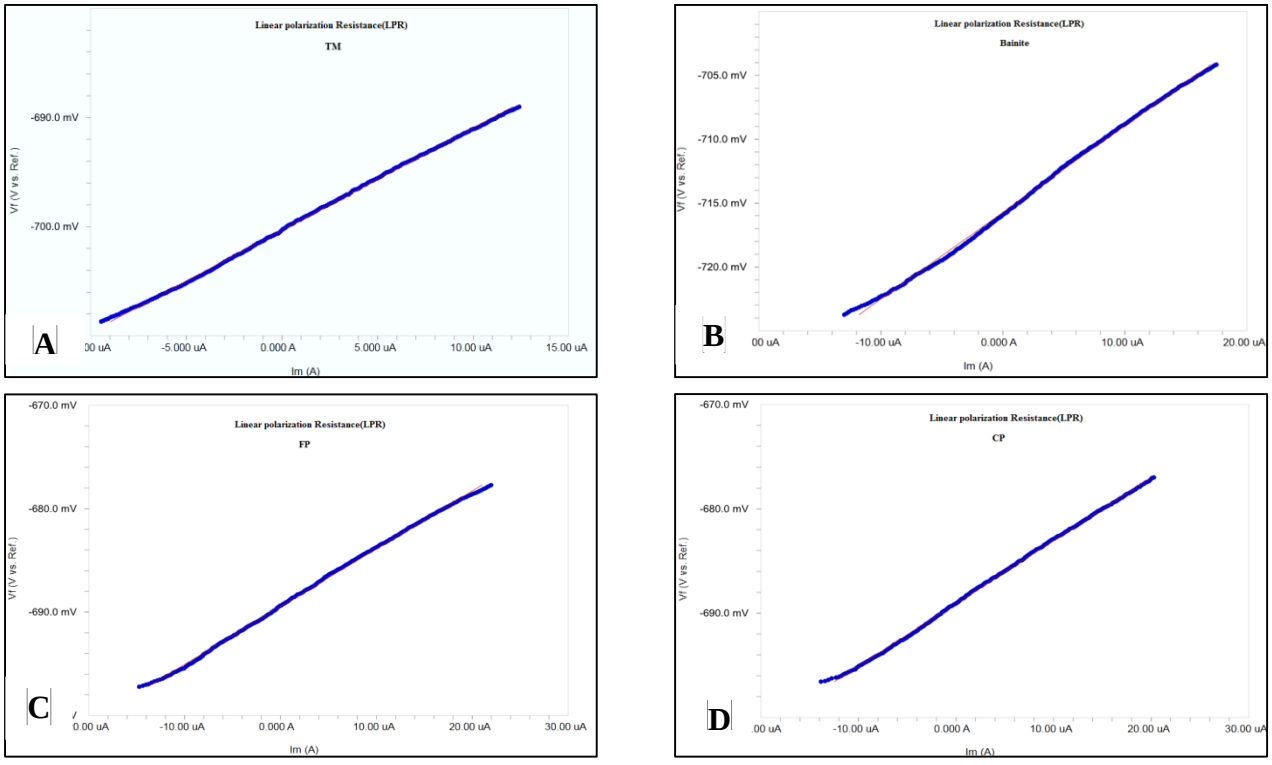

Figure 4.28: LPR Results (A) Tempered Martensite (B) Bainite B (C) Fine pearlite (D) Coarse pearlite

Table 4.13: Linear Polarization Resistance(LPR) of heat treated steel samples in 3.5% NaCl at room temperature.

	Icorr ($\mu A/cm^2$)	Ecorr(mV)	Rp(ohms)	Corrosion Rate(mpy)
TM	28	-700	930	16
Bainite	38	-716	679	22
fine pearlite	49	-689	528	28
course pearlite	43	-689	603	25

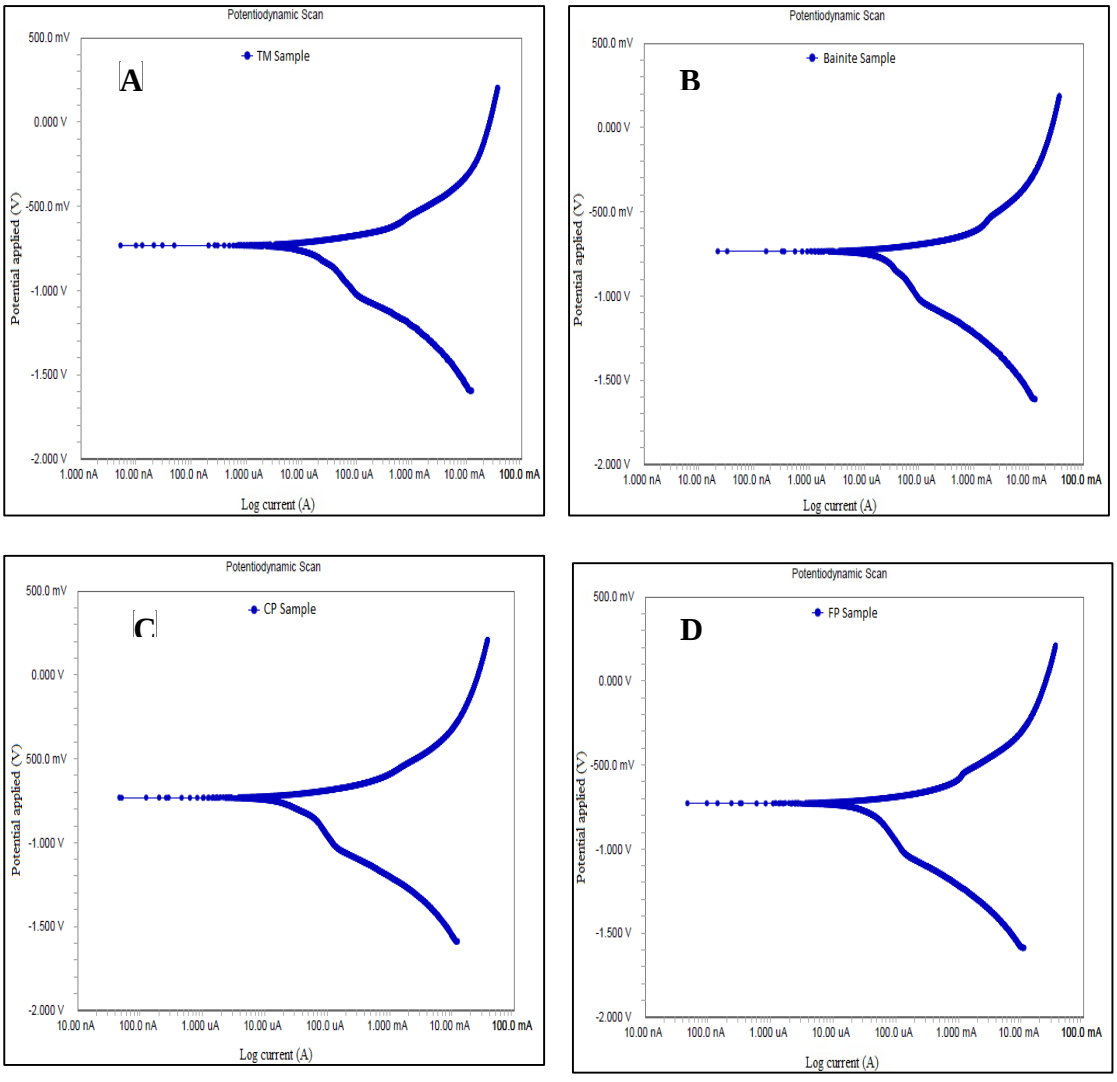

Figure 4.29: The polarization curves for heat treated steel Samples (Tempered martensite, Bainite, Fine perlite, and coarse pearlite) in 3.5% NaCl

So, the highest corrosion rates in terms of mpy were shown in all results fine pearlite the corrosion rate was 27 mpy. However, the electrochemical corrosion rates were found to decrease with Tempered martensite and the corrosion rate was 16 mpy. As mentioned earlier in previous section 4.1, the performance of Quenched rebar (Tempered martensite) in terms of corrosion rate was better than that of the Air cooling rebar in simulated solution concrete environment.

Understanding and the explanation of the previous result is related to microstructural observations. The explanation has been reported in the previous studies [26,38,39,40,41] that pearlite set up galvanic cells where the ferrite acts as anode and carbide acts as cathode, thus, the higher corrosion rates have been related to higher ferrite and carbide contents. In general the corrosion rate increased according to the following order of structures: (1) Tempered martensite, (2) Bainite Sample, (3) Coarse pearlite Sample and (4) Fine perlite Sample.

Similar behavior was also reported by [61] that the tempered martensite acts as a single phase. The presence of ferrite makes galvanic couple.

4.4.3 Comparison of corrosion behavior for different tempering temperatures

The steel samples were quenched and tempered at different temperatures by using Gleeble. The samples were tempered at 400 ^{0}C and 300 ^{0}C to see the effect of tempering temperatue on the corrosion resistance of quenched steel rebar. At the final stage of steel rebar production, the rebar moves inside a quench box. The quenching converts the rebar's surface layer to martensite and the core remains hot. Thus, heat flows from the rebar's center to its surface to form tempered martensite layer. Figure 4.30 shows the electrochemical impedance spectroscopy results comparing the corrosion behavior at two tempering temperatures after quenching

.

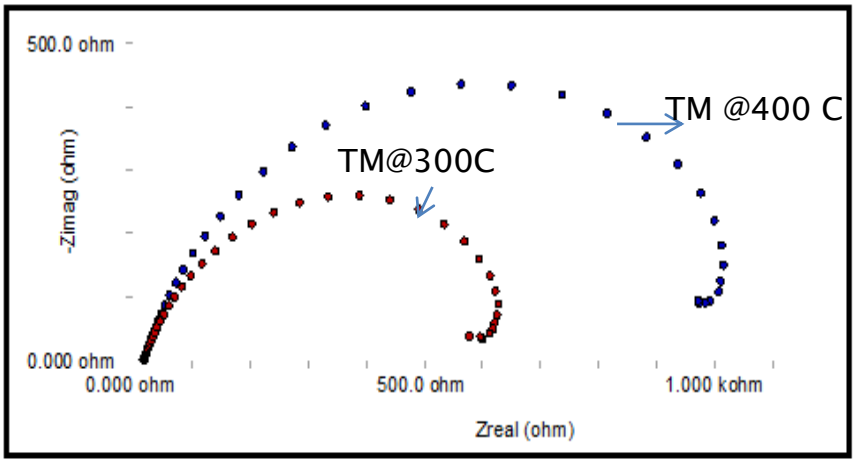

Figure 4.30: The electrochemical impedance spectroscopy (a) Tempered at 400 C and (b) Tempered at 300 C.

Figure 4.31 shows linear Polarization Resistance (LPR) comparison between the two tempering temperatures. The test was conducted at room temperature in 3.5% NaCl in order to study the corrosion behavior for two tempering temperatures after quenching.

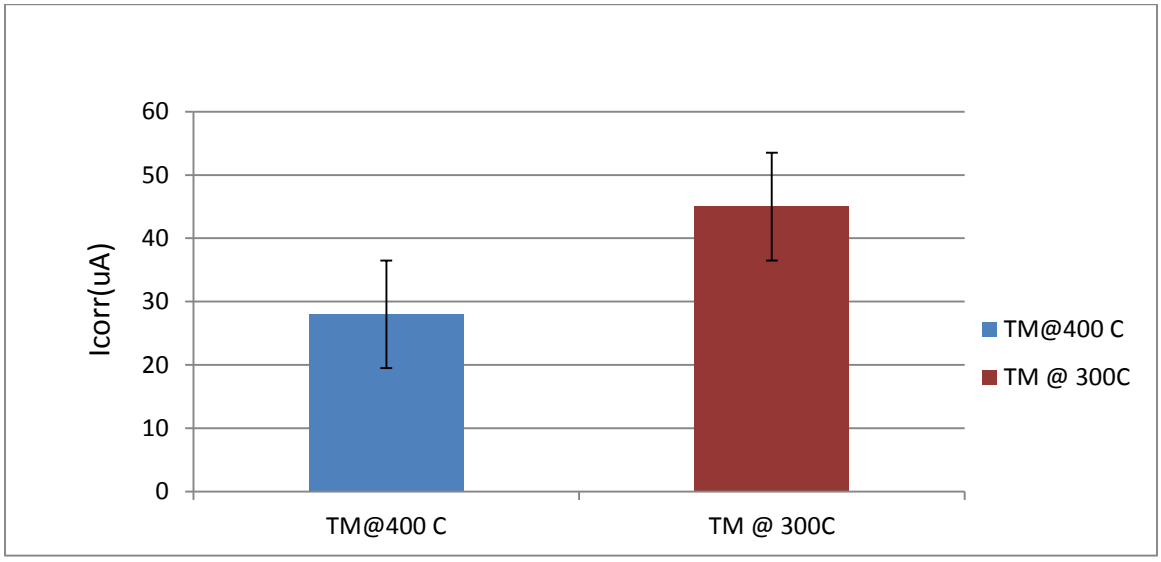

Figure 4.31: **LPR for two different tempering temperature in 3.5%NaCl.**

Figure 4.31 depicts corrosion current density for the two samples tempered at 400 ^{0}C and 300 ^{0}C. The corrosion current density (I_{corr}) of tempered martensite samples at 400 ^{0}C is lower than (I_{corr}) of TM at 300 ^{0}C. This shows that the TM at 400 ^{0}C has the higher corrosion resistance.

Table 4.14: Linear Polarization Resistance(LPR) of heat treated steel samples in 3.5% NaCl at room temperature.

Sample	AVG Icorr(uA)	Ecorr(mV)	Rp(ohms)	Corrosion Rate(mpy)
TM@400 C	28	-700	930.3	16.29
TM @ 300C	45	-675.1	695.1	21.8

CHAPTER 5

CONCLUSINS AND RECOMMENDATIONS

The objective of this project was to evaluate the corrosion resistance of steel rebar composition with different microstructures and to determine the relationships between microstructures and corrosion resistance of different steel rebars. Based on the experimental results developed in this investigation, The Important conclusions from this work are summarized below.

I. The corrosion resistance of different steel rebar

1. The corrosion resistance of Quenched and Tempered steel rebars (sample A, C, and D) is higher than the air-cooled steel rebar (sample B).
2. Comparison of corrosion resistance of Quenched and Tempered steel rebars reveal that sample A has the highest corrosion resistance, possibly due to high copper content

II. Effect of microstructure on the corrosion resistance of steel rebar

1. From Electrochemical impedance spectroscopy (EIS) results, it show that tempered martensite has the highest charge transfer resistance (Rct) value which is 1080 Ohm. This means tempered martensite has the highest corrosion resistance.
2. LPR, PDP and EIS reveal that the corrosion rate increased as shown in the results in the following order: (1) Tempered martensite, (2) Bainite Sample, (3) Coarse pearlite Sample and (4) Fine perlite Sample.
3. The corrosion current density I_{corr} of tempered martensite samples at 400 ^{0}C is lower than I_{corr} of tempered martensite at 300 ^{0}C.

References

1. Maslehuddin, M., Rasheeduzzafar, Page, C. L. Al-Mana, A. I., "Influence of Some Parameters Relevant to Arabian Gulf Environment on Reinforcement Corrosion," *Arabian Journal for Science and Engineering*: Theme Issue on Corrosion and its Prevention, April 1995, pp. 239-257.

2. Maslehuddin, M., Saricimen, H., Al-Mana, A. I., and Shamim, M., "Performance of Concrete in A High Chloride-Sulfate Environment," *American Concrete Institute, Special Publication SP-122*, 1990, pp. 469-494.

3. Saricimen, H., Al-Tayyib, A. J., Maslehuddin, M., Shamim, M., "Concrete Deterioration in High Chloride-Sulfate Environment and Repair Strategies," *American Concrete Institute, Special Publication, SP-128*, 1991, pp. 19-34.

4. Brent M. Phares, Fouad S. Fanous, Terry J. Wipf, Yoon-Si Lee, Milan J. Jolley "Evaluation of Corrosion Resistance of Different Steel Reinforcement Types" May 2006.

5. Saricimen H., "Concrete Durability Problems in the Arabian Gulf Region- A Review," Proceedings, Fourth International Conference Deterioration and Repair of R.C. in the Arabian, Gulf, Bahrain, 1993, pp. 943-959.

6. Shameem, M., Maslehuddin, M., Saricimen, H., and Al-Mana, A. I., "Extending the Life of Reinforced Concrete Structures in the Arabian Gulf Environment," Proceedings, Structural Faults and Repairs Conference, London, July 1995, pp. 115-126.

7. Chatterjee, Sponge Iron Production by Direct Reduction Of Iron Oxide, 2010.

8. Sankaran S, Subramanya SV, Padmanabhan KA. Low cycle fatigue behavior of multiphase microalloyed medium carbon steel: a comparison between ferrite– pearlite and quenched and tempered martensite microstructures. Mater Sci Eng A 2003;345:328–35.

9. Metals handbook metallography structures and phase diagrams, vol.8, 8th Edition, ASM. Handbook committee, Ed, By T. Lyman, American society of March, 1973.

10. D. R. Askeland , the science and Engineering of Materials , third Edition , monetary C.A, Brooks/Cole Engineering Division , 1994.
11. W.F. Smith , Foundations of Materials , Science and Engineering , 2nd Edition , New York , McGraw –hills , 1993, pp. 668-670.

12. W.D. Callister , Materials Science and Engineering , John Wiley and Sons 2007.

13. George Krauss, Steels: Processing, Structure, And Performance, August 30, 2005

14. Bo Yu, LuFeng Yang, Ming Wu, Bing Li, Practical model for predicting corrosion rate of steel reinforcement in concrete structures, Construction and Building Materials, Volume 54, 15 March 2014, Pages 385-401.

15. Z.P. Bazant, Physical Model for Steel Corrosion in Concrete Sea Structures Theory, ASCE J. Stru. Div., 105, 1979, p 1137–1153.

16. L. Bertolini, Corrosion of Reinforcement in Concrete Construction, Royal Society of Chemistry, Cambridge, 1996.

17. J.P. Broomfield, Corrosion of Steel in Concrete: Understanding, Investigation, and Repair, E & FN Spon, London, 1997.

18. K.C. Clear, Measuring the Rate of Corrosion of Steel in Field Concrete Structures, Transportation Research Record 1211, Transportation Research Board, National Research Council, Washington, DC, 1989.

19. G.G. Clemena and Y.P. Virmani, Comparing the Chloride Resistances of Reinforcing Bars: Evaluating New, Economical Metallic Reinforcementfor its Ability to Withstand High Salt Concentrations, Concr. Int.,2004, 26, p 39–49.

20. H.A.F. Dehwah, M. Maslehuddin, and S.A. Austin, Effect of Cement Alkalinity on Pore Solution Chemistry and Chloride-Induced Reinforcement Corrosion, ACI, Mater. J., 2002, 99(3), p 227–233.

21. S. Goni, and C. Andrade, Synthetic Concrete Pore Solution Chemistry and Rebar Corrosion Rate in the Presence of Chlorides, Cem. Concr.Res., 1990, 20, p 525–539.

22. M.F. Hurley, Corrosion Initiation and Propagation Behavior of Corrosion Resistant Concrete Reinforcing Materials. Doctoral dissertation.University of Virginia, Material Science and Engineering,Charlottesville, 2007.

23. T. Ishikawa, B. Bresler, and I. Cornet, Mechanism of Steel Corrosion inConcrete Structures, Mater. Prot., 1968, 7(3), p 45–47.

24. Maslehuddin, M. "Cathodic Protection Of Reinforcing Steel In Concrete" , March 2014.

25. ACI Committee 222, Protection of Metals in Concrete Against Corrosion, ACI 222R-01, American Concrete Institute, Farmington Hills, Michigan, 2001, 41 pages.

26. R. Winston Revie, Herbert H. Uhlig, An Introduction to Corrosion Science and Engineering, fourth edition,2008.

27. H. Cleary and N. D. Greene , Corros. Sci. 7 , 821 (1967).

28. M. Holmberg , Corrosion 2 , 278 (1946); R. Manuel , Corrosion 3 , 415 (1947).

29. Nedal Mohamed, Mohamed Boulfiza, and Richard Evitts, "Corrosion of Carbon Steel and Corrosion-Resistant Rebars in Concrete Structures Under Chloride Ion Attack", August 7, 2012.

30. L. Li and A.A. Sagues, Chloride Corrosion Threshold of Reinforcing Steel in Alkaline Solutions—Open-Circuit Immersion Tests, Corrosion,2001, 57(1), p 19.

31. P. Ghods a, O.B. Isgor a, G. McRae b, T. Miller ,"The effect of concrete pore solution composition on the quality of passive oxide films on black steel reinforcement", November 2008.

32. ASTM G 5-94. Standard reference test method for making potentiostatic and potentiodynamic anodic polarization measurements. West Conshohocken (PA): Annual Book of ASTM Standards; 2007.

33. Li L, Sagues AA. Chloride threshold of reinforcing steel in alkaline solutions –effect of specimen size. NACE Corros 2004;60(2):19–28.

34. J. Wei, J.H. Dong, W. Ke, The influence of cooling processes on the corrosion performance of the rebar scale, Construction and Building Materials, Volume 24, Issue 3, March 2010.

35. Wei J, Dong JH, Han EH, Ke W. Study on the corrosion resistance of hot rolled rebar quenched with a new chemical reagent, 2009.

36. E. Zitrou, J. Nikolaou, P.E. Tsakiridis, G.D. Papadimitriou, Atmospheric corrosion of steel reinforcing bars produced by various manufacturing processes, Construction and Building Materials, Volume 21, Issue 6, June 2007.

37. Groza JR, Eslamloo-Grami M, Bandy R. The effect of thermomechanical treatment on the pitting corrosion of reinforcing carbon steel bars. Werkst Korros 1993;44:359–66.

38. M Ismail, E Hamzah, GC Guan, I Abd Rahman ,Corrosion Performance of Dual Phase Steel Embedded in Concrete,Arabian Journal for Science and Engineering ,2010.

39. L.D. Paolinelli, T. Pérez, S.N. Simison, The effect of pre-corrosion and steel microstructure on inhibitor performance in CO2 corrosion, Corrosion Science, Volume 50, Issue 9, September 2008.

40. Lakshmana Rao Bhagavathi, G.P. Chaudhari, S.K. Nath, Mechanical and corrosion behavior of plain low carbon dual-phase steels, Materials & Design, Volume 32, Issue 1, January 2011.

41. Ramirez-Arteaga A. M., Gonzalez-Rodriguez J. G. , Campillo B. , Gaona- Tiburcio C., Dominguez-Patiño G., Leduc Lezama L. , Chacon-Nava J. G. , Neri- Flores M. A. and Martinez-VillafañeA." An Electrochemical Study of the Corrosion Behavior of a Dual Phase Steel in 0.5m H2SO4" , Int. J. Electrochem. Sci.,Vol. 5 (2010) PP. 1786 – 1798.

42. Damián A. López, S.N. Simison, S.R. de Sánchez, The influence of steel microstructure on CO2 corrosion. EIS studies on the inhibition efficiency of benzimidazole, Electrochimica Acta, Volume 48, Issue 7, 20 February 2003.

43. D. Clover1y, B. Kinsella1, B. Pejcic1 And R. De Marco, The influence of microstructure on the corrosion rate of various carbon steels, Journal of Applied Electrochemistry, Kluwer Academic Publishers 2005-02-01.

44. V. C. Igwemezie , J. E. O.Ovri , Investigation into the Effects of Microstructure on the Corrosion Susceptibility of Medium Carbon Steel, The International Journal Of Engineering And Science , 30.June.2013.

45. HOUYI MA1, SHENHAO CHEN*1,2, CHAO YANG3 and JINGLI LUO3, Comparison of the influence of nitrate ions on the electrochemical behaviour of iron and carbon steels in sulphate solutions, Department of Chemistry, Shandong University, 2002.

46. Asiful Hossain Seikh, Influence of Heat Treatment on the Corrosion of Microalloyed Steel in Sodium Chloride Solution, Hindawi Publishing Corporation, Journal of Chemistry Volume 2013.

47. M.A. Lucio-Garcia, J.G. Gonzalez-Rodriguez, M. Casales, L. Martinez, J.G. Chacon-Nava, M.A. Neri-Flores, A. Martinez-Villafañe, Effect of heat treatment on H2S corrosion of a micro-alloyed C–Mn steel, Corrosion Science, Volume 51, Issue 10, October 2009.

48. Oğuzhan Keleştemur, Servet Yıldız, Effect of various dual-phase heat treatments on the corrosion behavior of reinforcing steel used in the reinforced concrete structures, Construction and Building Materials, Volume 23, Issue 1, January 2009.

49. Sami I. Al-rubaiey , Eman A. Anoon and Mahdi M. Hanoon, The Influence of Microstructure on the Corrosion Rate of Carbon Steels, University of Technology/Baghdad, Eng. &Tech. Journal, Vol. 31,Part (A), No.10, 2013.
50. A.I. Zaky, A. El-Morsy, T. El-Bitar, Effect of different cooling rates on thermomechanically processed high-strength rebar steel, Journal of Materials Processing Technology, Volume 209, Issue 3, 1 February 2009.
51. Monideepa Mukherjee, Chaitali Dutta, Arunansu Haldar, Prediction of hardness of the tempered martensitic rim of TMT rebars, Materials Science and Engineering: A, Volume 543, 1 May 2012.
52. Stern, M., and Geary, A.L., 1957 "A Theoretical Analysis of the Slope of the Polarization," Curvesm Journal of The Electrochemical Society, Vol. 104, No. 1, pp. 56.
53. Mansfield, F., 1977 "Polarization Resistance Measurements: Experimental Procedure and Evaluation of Data", Electrochemical Techniques for Corrosion, NACE, Houston, pp. 18-26.
54. Gonzalez, A.J., Feliu, S., Andrade, C., and Rodriguez, I., 1991 "On-site Detection of Corrosion of Reinforced Concrete Structures, " Materials and Structures, Vol. 24, pp. 346-350.
55. Zhanli Guo*, Nigel Saunders, A. Peter Miodownik, Jean-Philippe Schillé, Introduction of Materials Modelling into Processing Simulation – Towards True Virtual Design and Simulation, International Journal of Metallurgical Engineering 2013.
56. L. Yu. Egorova, R. A. Savrai, V. V. Berezovskaya, A. V. Makarov, V. M. Schastlivtsev, T. I. Tabatchikova, E. A. Merkushkin, Relation between the structure and the pitting corrosion resistance of hypereutectoid U10 steel, Journal Article Russian Metallurgy, 2014.
57. V. M. Schastlivtsev, I. L. Yakovleva, and D. A. Mirzaev, "Structural transformations in pearlite during heating: I. Solidsolution hardening of the ferrite component of pearlite," Fiz. Met. Metalloved. 77 (4), 138–147(1994).
58. L. R. Bhagavathi, G. P. Chaudhari, and S. K. Nath,"Mechanical and corrosion behavior of plain low carbon dual phase steels," Mater. Design. 32, 433–440 (2011).
59. Ya. M. Kolotyrkin, Metal and Corrosion (Metallurgiya, Moscow, 1985).
60. Y.S. Tan, M.P. Srinivasan, S.O. Pehkonen, and S.Y.M. Chooi: Corrs. Sci. vol.48 (2006) p.840-862.

61. Zitrou E., Nikolaou J., Tsakiridis P. E., Papadimitiou G. D.: ‘Atmospheric corrosion of steels reinforcing bars produced by various manufacturing processes’, Construction and Building Materials, 2007, (21), 1161–1169.

Vitae

Name :Khaled Ayed ALQahtani

Nationality :Saudi Arabia

Date of Birth :10/5/1984

Email :khaled425@gmail.com

Address :P.O Box 11669 , Jubail 31961

Academic Background :Bachelor's degree in Mechanical Engineering from King Saud University in July 2009. My MS program at King Fahd University focused on materials and manufacturing engineering with different aspects of material properties, characterization, behavior and advanced analyses of manufacturing processes. . Part of my courses included corrosion monitoring, mechanical properties of engineering polymers and manufacturing. The extensive research work (as part of thesis) focuses on "The Effect of Microstructure on Corrosion Behavior of Steel rebar".